# 3

# Dehydration induced dynamical heterogeneity and ordering mechanism of lipid bilayers

## 3.1 INTRODUCTION

Lipid bilayers are essential components of cell membranes which act as semi-permeable boundaries between extra and intra-cellular environments. Lipid bilayers at fluid phase maintain the functionality of cells at physiological temperature [Milhaud, 2004]. The fluidity of the membrane is largely controlled by its hydration level or the water contents. Although the primary functions of membranes such as hosting trans-membrane proteins, exchange of bio-molecules for transport and drug-delivery are relevant at fully hydrated states for most organisms, a broad range of species can live under anhydrobiosis conditions over a long period of time [Tan *et al.*, 2015; Hamley, 2013]. The activity of anhydrous cell membranes in such organisms is important to their ability to avoid dissociation and is of tremendous biological importance [Crowe *et al.*, 1992]. Moreover, understanding biological membranes at low hydration levels are relevant for cryo-preservation techniques with large applications in food science, pharmacology, clinical medicine, and the preservation of human embryos for in-vitro fertilization [Trounson and Mohr, 1983; Crowe and Crowe, 2000].

Since water is a key parameter for the function and stability of membranes [Koster *et al.*, 1994; Gawrisch *et al.*, 1992; Stachura *et al.*, 2019], macroscopic architecture of membranes changes with the hydration numbers. With lowering in water content, phospholipid bilayers undergo into a more ordered state [Högberg and Lyubartsev, 2006]. Although water near bio and soft surfaces has received a lot of attention in the last decade [Persson and Halle, 2008; Jungwirth, 2015; Brzustowicz and Brunger, 2005; de Vries *et al.*, 2005a; Lin *et al.*, 2018; Pal *et al.*, 2002; Murzyn *et al.*, 2006], the physics of water and membrane dynamics correlation and its effect on the structure have not been fully explored yet. Therefore, the present study focuses on understanding the underlying dynamics that causes dehydration-directed fluid-to-gel crossovers of bilayers [Lin *et al.*, 2018; Högberg and Lyubartsev, 2006].

Recently, many experimental studies have shown the slow-down of water dynamics at lower hydration numbers near bilayers [Wassall, 1996; König *et al.*, 1994; Zhao *et al.*, 2008; Tielrooij *et al.*, 2009; Trapp *et al.*, 2010; Chen *et al.*, 2010; Mondal *et al.*, 2012; Yamamoto *et al.*, 2014; Ho *et al.*, 1995]. Thermodynamics of chain melting phase transition of diacylphosphatidylethanolamines obtained from calorimetric measurements as a function of water content has been studied. The free energy, enthalpy and entropy of phase transition have an tanh dependence on water content in terms of interlamellar water thickness and correlation length of water order [Cevc and Marsh, 1985]. Frequency modulation atomic force microscopy experiments show existence of two hydration layers near supported dipalmitoylphosphatidylcholine bilayers [Fukuma *et al.*, 2007]. Using dynamic atomic force microscope technique in association with a carbon nanotube probe, it has been shown that the hydration force and molecular ordering of water can be modified by changing

the membrane fluidity [Higgins *et al.*, 2006]. Dynamical experiments have shown columner order in liquid crystalline phases of stacked lipid bilayers due to the coupling between two-dimensional intralayer domain growth and interlayer smectic ordering [Tayebi *et al.*, 2012]assisted by solvents. Using infrared spectroscopy, an increased fraction of well structured, low density network water has been observed near the POPC bilayer upon dehydration similar to super-cooled water near $-25^0$C [Binder, 2007]. Nuclear magnetic resonance (NMR) spectroscopy has shown that the water diffusion near egg PC-water system, DOPC and POPC bilayer system depends on change in hydration number [Wassall, 1996; König *et al.*, 1994]. Using ultrafast polarization selective vibrational spectroscopy, a slow down in orientational relaxation of water has been observed near artificial multibilayers of the phospholipid dilauroyl phosphatidylcholine DLPC as the hydration of water decreases [Zhao *et al.*, 2008]. Two major types of interfacial water molecules are found: one clathrate-like cluster associated with choline moieties and the hydration water near phosphate groups. Using terahertz spectroscopy it has been found that the bulk-like water dynamics slowly disappear at a lower hydration level and a fast and slow reorienting water molecules appear [Tielrooij *et al.*, 2009]. Using neutron scattering experiments [Trapp *et al.*, 2010], the effect of hydration numbers on DMPC bilayers above and below the main phase transition temperature is recorded. Quasielastic neutron scattering experiments (QENS)[Doxastakis *et al.*, 2007] and simulations have been performed for 1,2-Dipalmitoyl-sn-glycero-3-phosphocholine (DPPC) bilayer at low hydration number. It is observed that the melting of the bilayer occurs at higher temperature at lower hydration due to the packing of the bilayer.

Complementary to the experiments, molecular dynamics (MD) simulations have been performed to understand the structural and dynamical properties of water at microscopic level. Reorientatioanl auto correlation function (RACF) is calculated to understand the orientation of water molecule near bilayer surface on varying the hydration number. Water relaxation time increases from high to low water contents [Calero and Franzese, 2019; Stachura *et al.*, 2019; Högberg and Lyubartsev, 2006; Calero *et al.*, 2016]. Interfacial water (IW) near phopholipid bilayer are very strongly bound via hydrogen bonds(HBs) to the polar groups of the lipid bilayer [Calero and Franzese, 2019]. For DMPC as well as for DOPC bilayers, diffusion of the IW slows down on lowering the hydration number [Stachura *et al.*, 2019; Högberg and Lyubartsev, 2006]. Bilayers become more ordered as the number of water molecules per lipid decreases. The order parameter, area per head group and thickness of DMPC, DOPC, POPC bilayers confirm that the fluid phase changes to a gel phase as water per lipid is lowered to $\sim 10$. Similar to the slow down of the IW near bilayer phase change, slow down of the IW are found near dynamical cross-overs of proteins or cryoprotecting biolomolecules using MD simulations and neutron scattering experiments [Wood *et al.*, 2008; Iorio *et al.*, 2019]. The changes in bilayer structure and the slow-down of water dynamics induced by dehydration are clearly observed in previous experiments and simulations. Although the interplay between the water dynamics and the ordering of membranes upon lowering water contents have been investigated in previous molecular dynamics study [Högberg and Lyubartsev, 2006], the relation of growing relaxation time-scales of interface water with dehydration and its effect on the spatial distributions of the local dynamics of membranes remain unattended so far.

The present study reveals the relation between slow relaxation of the interface water to dynamical heterogeneity when water content is lowered. The objective of the work is to find out how dehydration induces dynamical heterogeneity in the interface water and how the heterogeneous coupled dynamics of the interface water and the local lipids influences the bilayer ordering. To this end, we have performed all-atom MD simulations at different water contents near dimyristoylphosphatidylcholine (DMPC) bilayers. To understand the dynamical properties of water near the bilayer, translational mean square displacements (MSD) of IW are calculated for

various water contents. A plateau like behavior in MSD has indicated the emergence of dynamical heterogeneity in IW upon dehydration. To confirm the existence of dynamical heterogeneity upon dehydration, non-Gaussian parameters (NGP), 1D van-Hove correlation functions, self-intermediate scattering functions (SISF) are calculated for the IW. Relations between diffusion constant and $\alpha$ relaxation times are analyzed at different water contents. Hydrogen bond auto correlation function and reorientation of auto correlation (RACF) of IW are calculated. To establish the correlation between dynamical heterogeneity and bilayer fluid-to-gel crossover, order parameter, area per lipids, 2D van Hove correlation functions of bilayers are calculated. Our results show that the dynamical heterogeneity arises in the IW as well as in the bilayer upon lowering the water contents. The emergence of dynamical heterogeneity leads to the chain ordering of the bilayer at room temperature. Thus the work provides the mechanistic insights to the dehydration induced bilayer ordering.

## 3.2 SIMULATION DETAILS

Figure 3.1 (a) shows the structure of a DMPC molecule. An equilibrated configuration of a fully hydrated bilayer with 128 DMPC molecules in presence of 5743 TIP4P/2005 [Abascal and Vega, 2005; Srivastava *et al.*, 2019a] water molecules is used as the starting configuration (figure 3.1 b)) to generate bilayers with different water contents. CHARMM36 [Klauda *et al.*, 2010] force fields are used for DMPC bilayers. CHARMM36 in combination with TIP4P/2005 is known to work well for calculating water dynamics near a membrane at the fluid phase [Srivastava *et al.*, 2019a; Kučerka *et al.*, 2011; Zhuang *et al.*, 2014]. The fully hydrated bilayer corresponds to $\omega = 45$, where $\omega$ represents the water content or the hydration number. At $\omega = 45$, the bilayer is in fluid phase as previously reported in experiments [Lopez *et al.*, 2004; Zhao *et al.*, 2008; Trapp *et al.*, 2010; Nagle *et al.*, 1996]. Figure 3.2 shows that the fully hydrated bilayer reaches diffusive regime confirming the fluid phase. Eight different bilayers are generated from the equilibrated bilayer where $\omega$ ranges from 45 to 4 ($45, 35, 32, 26, 18, 10, 8, 6$ and 4) at 308K (table 3.1). Figure 3.1 c) shows the equilibrated bilayer with $\omega = 4$. GROMACS-4.6.5 [Bekker *et al.*, 1993; Berendsen *et al.*, 1995; Lindahl *et al.*, 2001; Van Der Spoel *et al.*, 2005; Hess *et al.*, 2008] software package is used to conduct these simulations. All bilayers in table 3.1 are equilibrated at 308 K temperature

**Table 3.1 :** Details of the systems studied.

| Hydration number, $\omega$ | Water molecules | Box Size, nm |
|---|---|---|
| 45 | 5743 | $6.27 \times 6.27 \times 7.90$ |
| 35 | 4480 | $6.35 \times 6.35 \times 6.75$ |
| 32 | 4096 | $6.34 \times 6.34 \times 6.49$ |
| 26 | 3328 | $6.29 \times 6.295.02$ |
| 18 | 2304 | $6.41 \times 6.41 \times 5.02$ |
| 10 | 1331 | $6.22 \times 6.22 \times 4.69$ |
| 8 | 1024 | $6.05 \times 6.05 \times 4.60$ |
| 6 | 768 | $5.92 \times 5.92 \times 4.57$ |
| 4 | 512 | $5.77 \times 5.77 \times 4.56$ |
| 45 | 51687 | $18.27 \times 18.27 \times 7.90$ |
| 4 | 4608 | $17.37 \times 17.37 \times 4.56$ |

using the Berendsen method [Berendsen *et al.*, 1984] with a coupling constant of 0.5 ps in NPT ensembles with a time step of 2 fs. Semi-isotropic pressure coupling is applied using Berendsen

method [Berendsen *et al.*, 1984] to maintain the pressure of 1 bar with compressibility factors of $4.5 \times 10^{-5}$ bar$^{-1}$ and coupling constants of 1.0 ps independently in xy and z directions. Here, the changes in the x-y dimensions are independent of the ones along the z-axis. Cutoff 1.2 nm is used for van der Waals interactions. For electrostatic interactions, the Particle Mesh Ewald approach [Darden *et al.*, 1993; Essmann *et al.*, 1995; de Vries *et al.*, 2005a] is used. Periodic boundary conditions are applied in xyz directions. Thus the simulated bilayers are multilamellar stack, due to the periodic boundary conditions. LINCS [Hess *et al.*, 1997] algorithm is used to keep bonds with hydrogens constant. The equilibration period in the NPT ensemble is 550 ns for $\omega = 45$ and 100 ns for remaining systems. System sizes of the equilibrated bilayers are mentioned in the table 3.1. Next, NVT runs are performed for 1 ns with a 0.4 fs time step and a 10 fs saving frequency without constraints for all bilayers. Nosé-Hoover temperature coupling is used to maintain the temperature of 308 K with a coupling constant of 0.5 ps. Long and short-range distance corrections for the NVT runs are same as for the NPT runs. Center of mass motions are removed during the NVT production runs. Different run-lengths are used for different dynamical calculations to obtain good statistics as such high frequency runs are expensive for the all atom MD simulations of the bilayers.

Additionally a bulk water (BW) system consisting of 851 water molecules is simulated using TIP4P/2005 water model at 308 K to compare water dynamics with dynamics of IW near bilayers with different water contents.

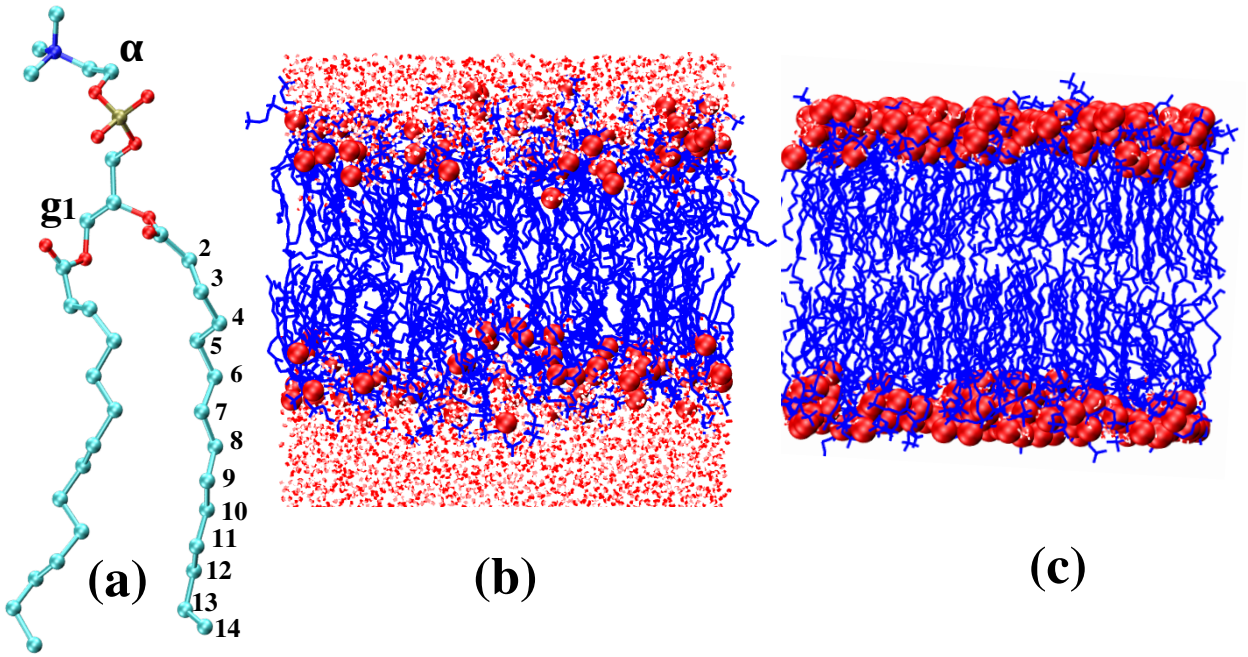


**Figure 3.1 :** Snapshot of (a) a DMPC molecule (explicit hydrogen atoms are not shown for the purpose of the clarity), DMPC bilayer for (b) $\omega = 44$ and (c) $\omega = 4$. Color code with representation: DMPC: CPK (Corey-Pauling-Koltun) representation in blue; Water: red; IW water: VDW (van der Waals) representation in red.

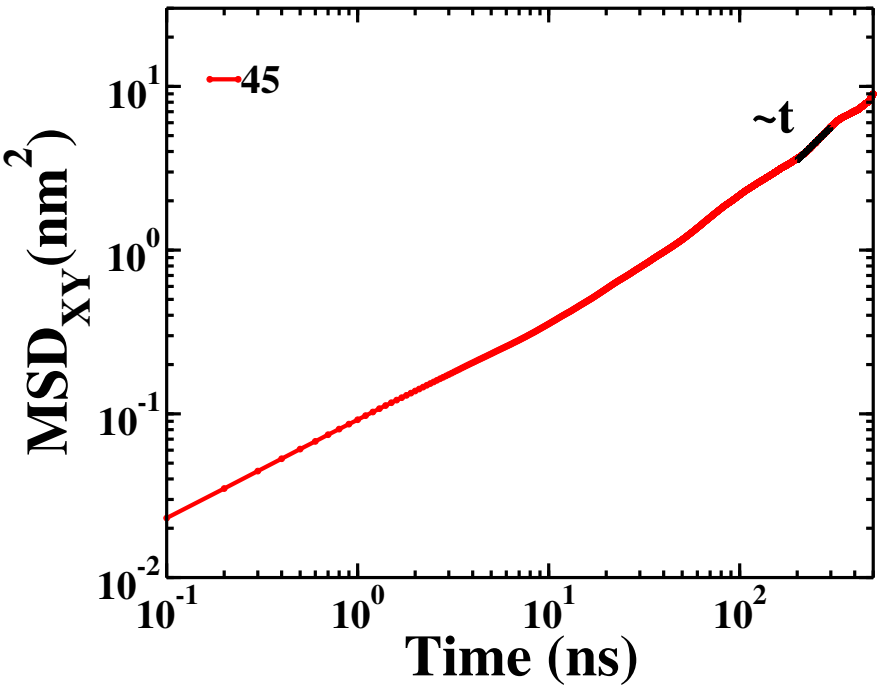


**Figure 3.2 :** Mean square displacements of phosphorous heads of bilayer at $\omega = 45$ showing the lipid reaches diffusive regime near 200 ns.

## 3.3 RESULTS AND DISCUSSIONS

### 3.3.1 Structural properties of lipid bilayers upon dehydration

To investigate the effect of dehydration on the lateral organization of bilayers, area per lipid ($a_h$) of the bilayers are calculated by,

$$a_h = \left\langle \frac{b_x b_y}{N_l} \right\rangle, \tag{3.1}$$

where, $b_x$ and $b_y$ are box lengths along x and y directions respectively, $N_l$ denotes number of lipids in one leaflet, angular brackets denote the time average. Figure 3.3 shows the time evolution of area per lipid for different $\omega$. Figure 3.4 a) shows $a_h$ of the bilayer falls off from $\omega = 10-4$. Our results agree well with the area per lipid of different lipids obtained from different force-fields [Stachura *et al.*, 2019; Högberg and Lyubartsev, 2006]. The lowering in $a_h$ from $\omega = 10-4$ indicates a chain ordering crossover in bilayer at 308 K. The value of area per lipid from $\omega = 45$ to 4 is between fluid and gel phases (table 3.2) which might indicate the existence of the ordered phase at lower $\omega$.

Thickness of bilayers ($D_{HH}$) is calculated using the following equation,

$$D_{HH} = \langle Z_l \rangle - \langle Z_u \rangle, \tag{3.2}$$

where, $\langle Z_l \rangle$ and $\langle Z_u \rangle$ are time-averaged z-coordinates of the phosphorous heads obtained from the respective density profiles figure 3.7. Similar to the $a_h$, bilayer thickness remains constant above $\omega = 10$ and then increases as hydration number decreases (figure 3.4 b)). Changes in both $a_h$ and $D_{HH}$ from $\omega = 10-4$ indicate a crossover in bilayers due to dehydration. Our results show that

**Table 3.2 :** Comparison of fully hydrated and dehydrated DMPC bilayers at 308 K from our simulations with fully hydrated fluid and gel phases at different temperatures from literature.

| Properties | $\omega$ | our simulation ($308K$) | Literature | |
|---|---|---|---|---|
| | | | Simulation | Experiment |
| $a_h(\mathrm{nm}^2)$ | 45 | $0.62 \pm 0.01$ | $0.60 \pm 0.02$ [Zhuang *et al.*, 2014] (303K), fluid | $0.599 \pm 0.12$ [Kučerka *et al.*, 2011] (303K), fluid |
| | 4 | $0.52 \pm 0.03$ | $0.50 \pm 0.03$ [Khakbaz and Klauda, 2018] (273K), gel | $0.472 \pm 0.05$ [Tristram-Nagle *et al.*, 2002] (283K), gel |
| $D_{HH}(\mathrm{nm})$ | 45 | 3.5 | 3.62 [Zhuang *et al.*, 2014] (303K), fluid | $3.6 \pm 0.02$ [Kučerka *et al.*, 2011] (303K), fluid |
| | 4 | 4.01 | $4.04 \pm 0.05$ [Khakbaz and Klauda, 2018] (273 K), fluid | $4.01 \pm 0.01$ [Tristram-Nagle *et al.*, 2002] (283K), gel |
| $\lvert S_{CD} \rvert$ | 45 | $0.19 \pm 0.03$ | $0.195 \pm 0.03$ [Srivastava *et al.*, 2019a] (308K), fluid | 0.18 [Srivastava *et al.*, 2019a] (303K), fluid |
| | 4 | $0.26 \pm 0.02$ | $0.25 \pm 0.02$ [Khakbaz and Klauda, 2018] (273K), gel | - |

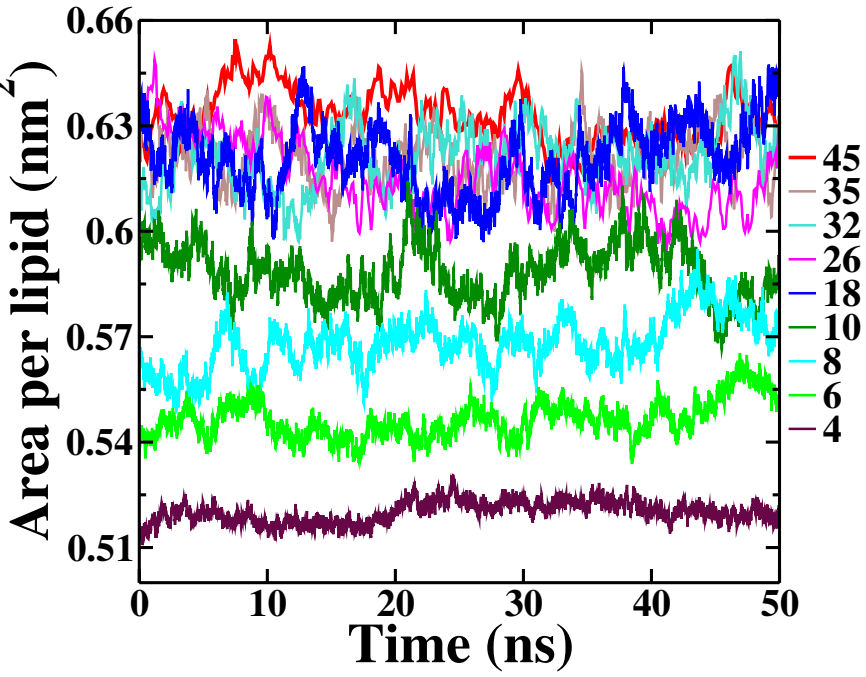


**Figure 3.3 :** Area per head group of lipids at different $\omega$ during production runs.

ordering in DMPC bilayer start at $\omega = 10$ at 308 K and the ordering increases till $\omega = 4$. For DOPC lipids with CHARMM force-fields and DMPC lipids with GROMOS force-fields similar crossover happen at $\omega \sim 18$ and 10 respectively [Stachura *et al.*, 2019; Högberg and Lyubartsev, 2006]. Our results are in good agreement with the experimental values [Kučerka *et al.*, 2011; Nagle *et al.*, 1996] mentioned in table 3.2.

To investigate the alignment of chains with respect to the bilayer normal, order parameter,$|S_{CD}|$ [Vermeer *et al.*, 2007; Högberg and Lyubartsev, 2006] has been calculated using following equation,

$$|S_{CD}| = \frac{1}{2} < 3cos^2\theta - 1 >, \tag{3.3}$$

where $\theta$ is the angle between the bilayer normal and the C-H vector. Angular brackets denote an average over time and molecule. Figure 3.5 a) depicts the order parameter of DMPC chains with respect to the carbon number along the alkyl chains from $\omega = 45$ to 4. Figure 3.5 b) shows the changes of order parameter averaged over the carbon numbers along the alkyl chain with $\omega$. Distributions of angles between CH vectors and the bilayer normal are calculated for different CH along the chain and shown in figure 3.6. The distribution becomes narrower from $\omega = 45$ to 4 with a shift in peaks for $\alpha$ CH and glyc. CH. Similar trend has been observed in previous simulations [Högberg and Lyubartsev, 2006]. The distribution is moderately narrower from 45 to 4 without any shift in peak for tail 4 and 14 CH. Thus the degree of ordering upon dehydration is more prominent in the tail 4 and 14 CH than that in the $\alpha$ CH or glyc. CH. Importantly, the peaks of the angle distributions of the head to tail vector with the bilayer normal becomes significantly narrower from 45 to 4 near 15° suggesting a crossover in chain ordering from high to low $\omega$.

Table3.2 represents the comparison of our results with existing literature from simulations and experiments for $\omega = 45$ and 4. The values of $a_h$, $D_{HH}$ and $|S_{CD}|$ at $\omega = 45$ from our calculations

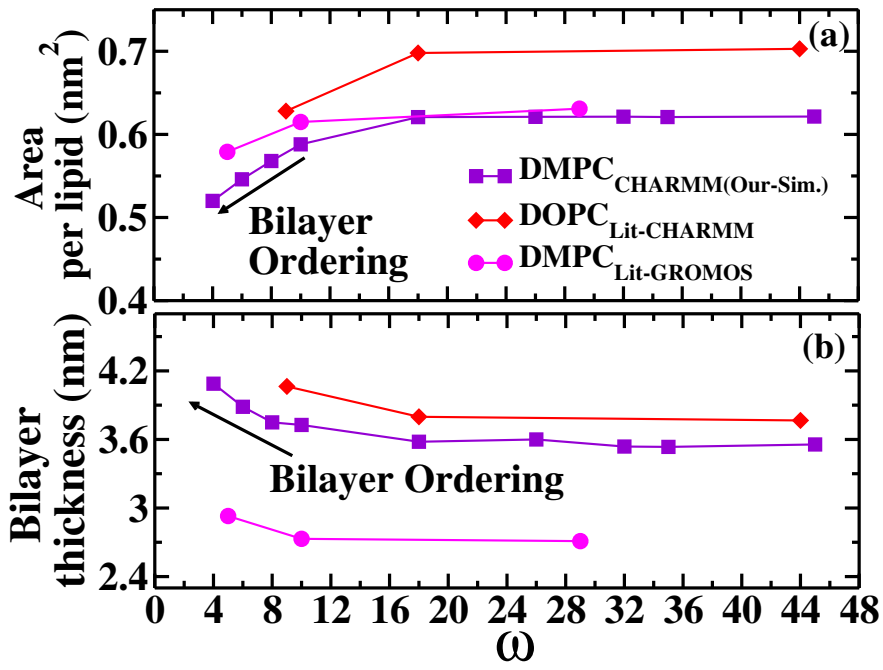


**Figure 3.4 :** (a) Area per lipid and (b) Bilayer thickness with change in hydration number for DMPC$_{CHARMM(our-sim.)}$, DOPC$_{Lit-CHAMRMM}$ [Stachura *et al.*, 2019] and DMPC$_{Lit-GROMOS}$[Högberg and Lyubartsev, 2006]. Decrease in area per lipid and increase in bilayer thickness are found from $\omega = 10 - 4$.

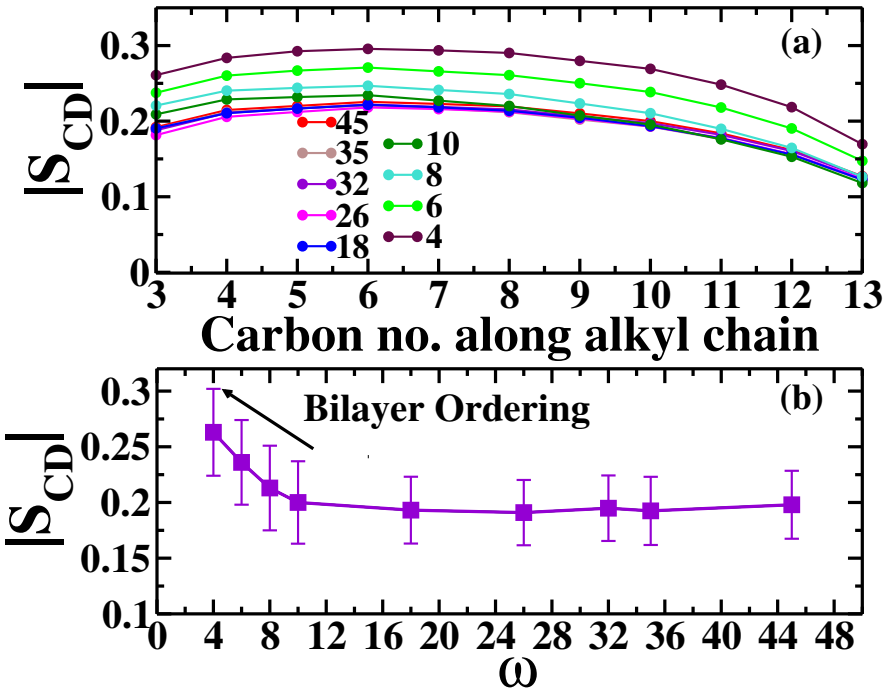


**Figure 3.5 :** (a) Order parameter with respect to atom number along the alkyl chain and b) Averaged order parameter with respect to $\omega$ from 45 to 4. $S_{CD}$ increases from $\omega = 10 - 4$.

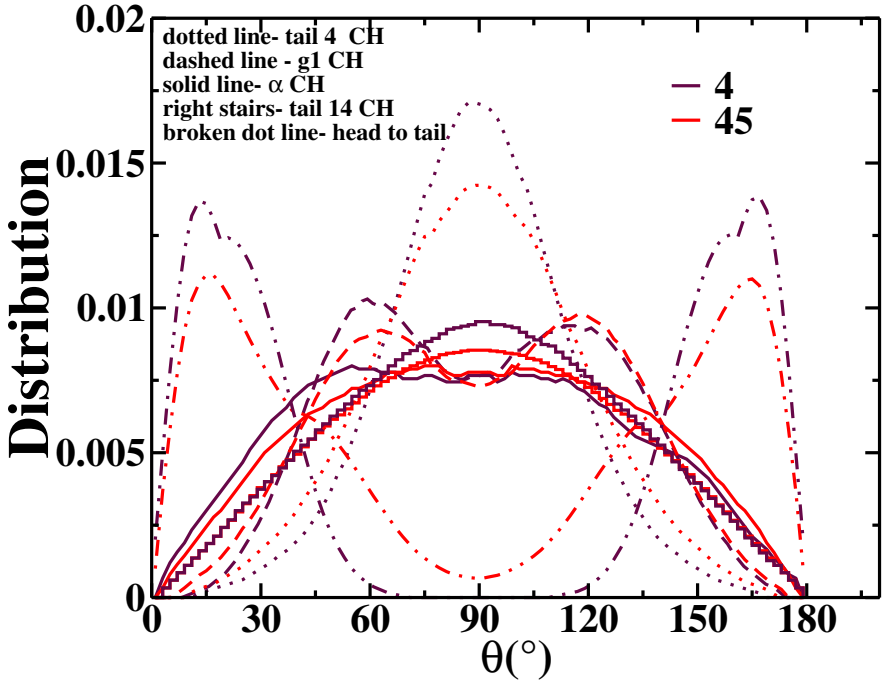


**Figure 3.6 :** Distribution of angles between CH vectors and the bilayer normal for hydration number 45 and 4. Solid lines: CH, dashed line: Glyc. CH and dotted lines: tail 4 CH, right stairs: tail 14 CH, broken dot lines: head (phosphorous) to tail (14 C) vector.

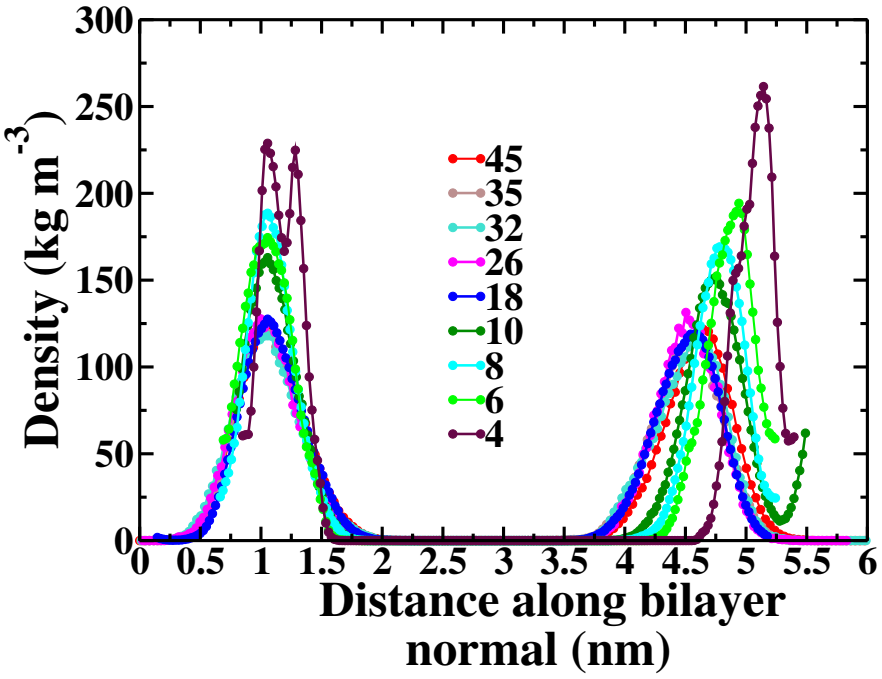


**Figure 3.7 :** Density profile of lipid heads at different $\omega$.

match well with the ones at a fluid phase obtained from simulation and experiments. Similarly, these values from our calculations at $\omega = 4$ match well with the ones at a gel phase. Thus by comparing the values of $a_h$, $D_{HH}$ and $|S_{CD}|$, bilayers at the full and least hydrations are identified as fluid and gel bilayers respectively. Our analyses show that, the bilayer has undergone a fluid-to-gel crossover when the water content is near $\omega = 10$. This is consistent with previous molecular dynamics finding of bilayer undergoing into more ordered state upon lowering water contents [Högberg and Lyubartsev, 2006].

The thickness of the bilayer is calculated as a function of the bilayer surface, $(x,y)$, as follows,

$$t(x,y) = \langle z_l(x,y) - z_u(x,y) \rangle \,. \tag{3.4}$$

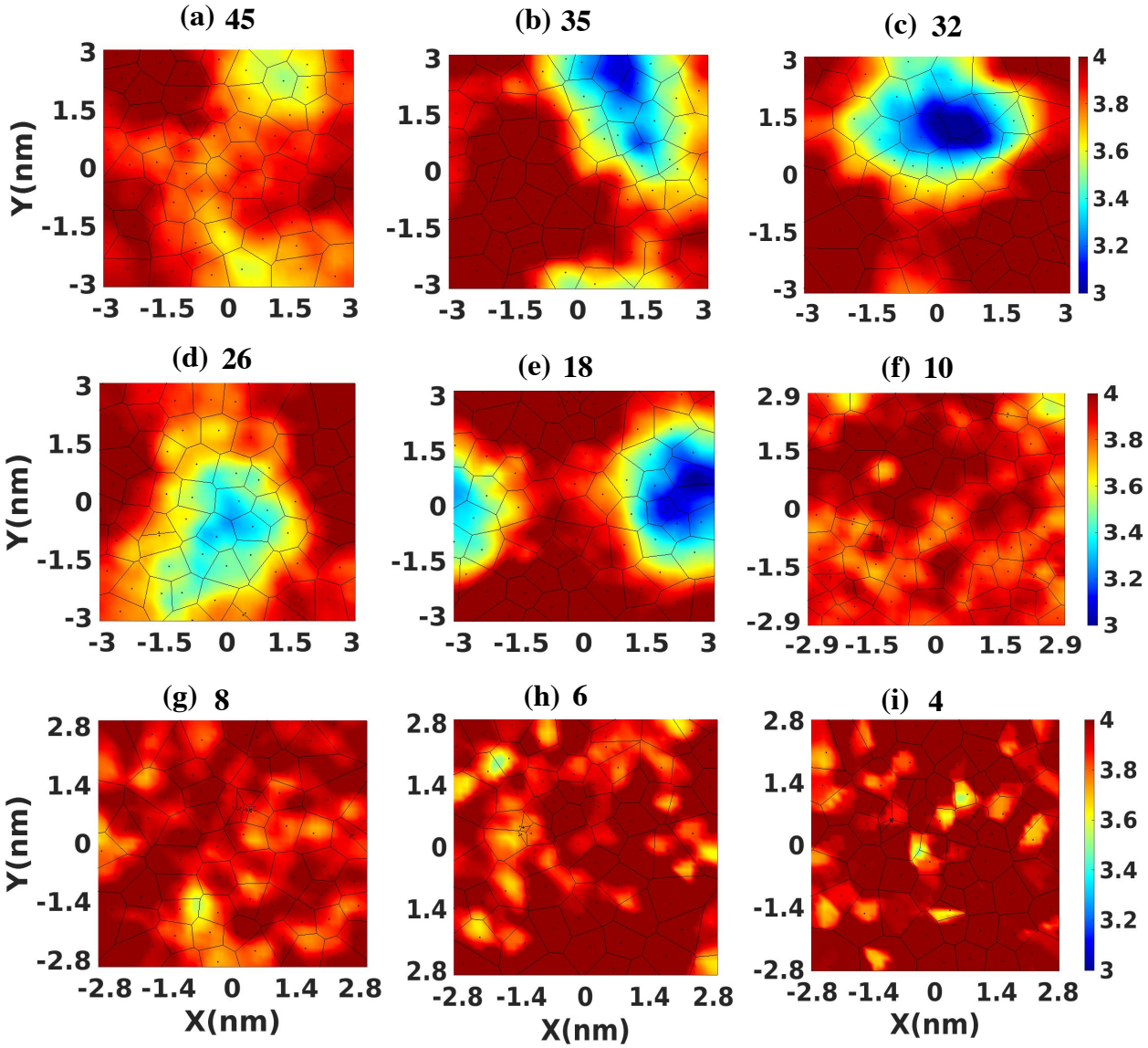


**Figure 3.8 :** Thickness superimposed on Voronoi area per lipid head from hydration number a) 45 to i) 4. The colorbar is in nm. The bilayer undergoes a fluid-to-gel crossover with lowering in water contents.

$z_l(x,y)$ and $z_u(x,y)$ are the $z$ co-ordinates of the lipid head groups for the lower and the upper leaflets respectively as functions of bilayer surface, $(x,y)$. Angular brackets denote averaging over time. The thicknesses $t(x,y)$ are superimposed on the Voronoi area per lipid [Debnath *et al.*, 2014] for all hydration states using MATLAB.

At $\omega = 45$, the thickness of the bilayer is $3.6-4$ nm which varies a little (within $0.3-0.4$ nm) indicating the fluid or liquid crystalline phase at the full hydration state (figure 3.8 a)). With lowering in $\omega$, small domains of lower thicknesses arise in the bilayers which remain stable above $\omega = 10$ (figure 3.8 b)-e)). On lowering $\omega$ below 10, the variations in thickness on the bilayer surface disappear and the thicknesses increase indicating chain ordering. Such homogeneous distributions of higher thickness of the bilayers remain stable till the lowest hydration number 4 demonstrating the existence of a gel phase at the lowest hydration. The thicknesses superimposed on the Voronoi area per lipid clearly show that for intermediate hydrated states, $\omega = 35$ to 18, the bilayers have nano-sized regions or domains with lower and higher thicknesses.

To understand the structure of nano-domains better, interdigitation of chains are calculated as a function of surface $(x,y)$ as follows

$$I(x,y) = z_{l,end} - z_{u,end}, \tag{3.5}$$

where $z_{l,end}$ and $z_{u,end}$ are the $z$ coordinates of the end beads of lower and upper leaflets respectively. A comparison of the locations of the regions with lower thickness and interdigitation (figure 3.9) reveals that the nano-domains with lower thicknesses correspond to interdigitated chains (hydration number $45-18$). The thickness increases in the gel phase and the interdigitation disappears. This represents bilayers have regions with co-existence of ordered and disordered chains above $\omega = 10$. From $\omega = 10$, lipids start ordering by increasing the bilayer thickness and the bilayer undergoes a fluid to a gel crossover near $\omega = 10$.

### 3.3.2 Dynamical properties of IW

#### *Survival Probability of IW*

Survival probabilities of water molecules near bilayers with different hydration numbers are computed using the following equation,

$$S(t) = \sum_{i=1}^{N} <_{t_k=t_0}^{t_0+t} P_i(t_k) > \tag{3.6}$$

where $S(t)$ is the probability of finding a water molecule residing in the interface layer at time $t$. $N$ represents total number of molecules, angular bracket represents averaging over time origins $t_0$. $P_i(t) = 1$ if the molecule is present in the interface layer at time t and $P_i(t) = 0$ otherwise. Figure 3.10 represents the survival probabilities of water near membranes at a fully hydrated state ( $\omega = 45$) and at a dehydrated state ($\omega = 4$). The decay for $\omega = 4$ is slowest showing the highest survival probability of water upon dehydration. The residence time scales for the interface water are extracted by fitting the normalized survival probability to bi or tri-exponential functions given by following equation,

$$y = A_f exp(-t/\tau_f) + A_i exp(-t/\tau_i) + A_s exp(-t/\tau_s) \tag{3.7}$$

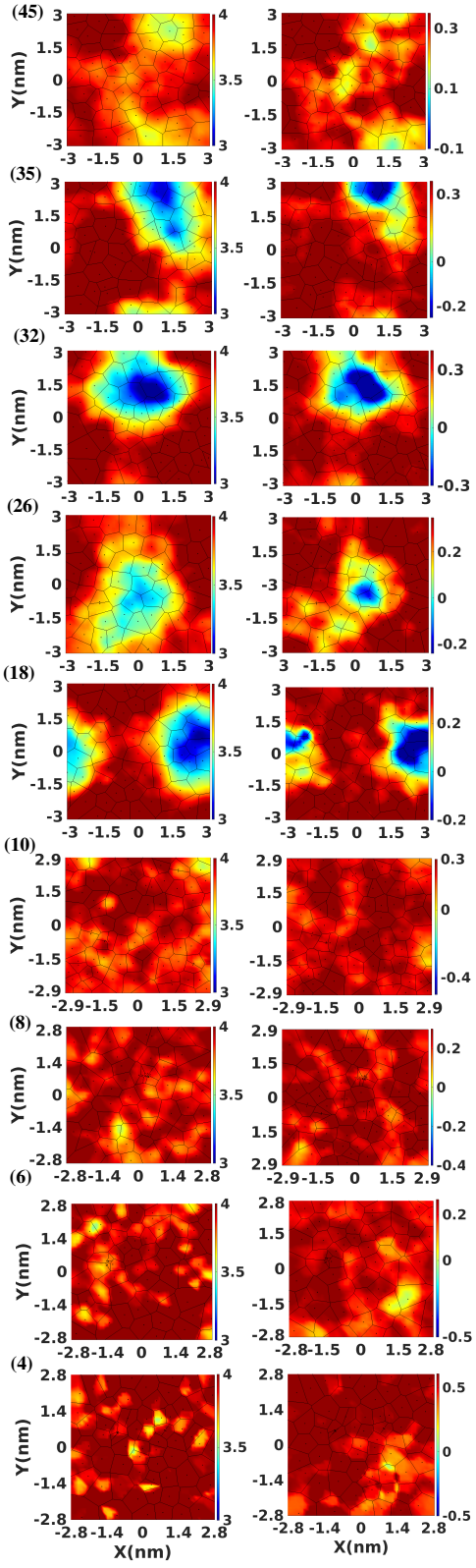


**Figure 3.9 :** Left panel: Thickness and right panel: Interdigitation superimposed in voronoi area per lipid head from hydration number 45 to 4.

Interfacial water show two or three characteristic time scales for $\omega = 45$ and 4 respectively. $\tau_f$, $\tau_i$ and $\tau_s$ represent fast, intermediate and slow time scales. The extracted timescales ($\tau_f$, $\tau_i$ and

**Table 3.3 :** Fitted parameters to survival probability of water computed over 1 ns and 10 ns with a saving frequency of 1 ps for hydration number 45 and 4 respectively.

| $\omega$ | $A_f$ | $\tau_f$ (ps) | $A_i$ | $\tau_i$ (ps) | $A_s$ | $\tau_s$ (ps) |
|---|---|---|---|---|---|---|
| 45 | 0.40 | 20.01 | - | - | 0.49 | 123 |
| 4 | 0.30 | 29.16 | 0.24 | 448 | 0.27 | 2621 |

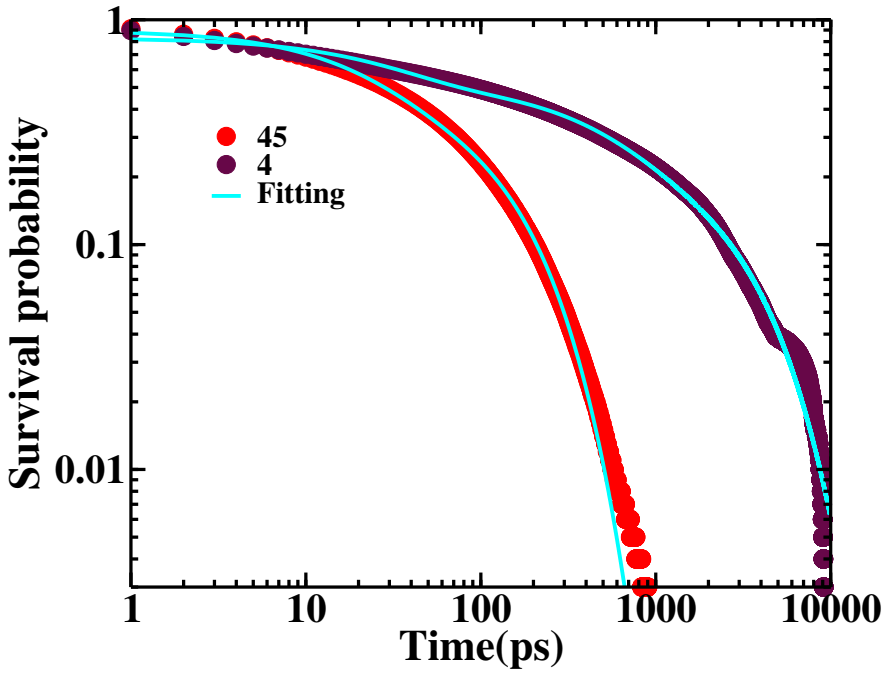


**Figure 3.10 :** Survival probability of water molecules for hydration number 45 and 4. Black solid lines show bi-exponential fitting.

$\tau_s$) and the coefficients ($A_s$, $A_i$ and $A_f$ ) from the fitting are presented in table 3.3. Since the $S(t)$ of water decays completely, $\tau_s$ represents the residence time. From the fitting parameters shown in table S1, it has been found that residence times ($\tau_s$) of water near the bilayers with hydration numbers 45 and 4 are 123 ps and $\sim 2621$ ps respectively. Since the water dynamics for $\omega = 45$ is fastest among all hydration numbers and 123 ps is the residence time of the interface water for the highest $\omega$, residence time of water for lower hydration numbers should be above 123 ps. Therefore, 100 ps is chosen as the confinement lifetime as this timescale is obeyed by interface water for all hydration numbers. Previously 100 ps is found to be the residence time for IW [Srivastava *et al.*, 2020; Debnath *et al.*, 2010].

IW molecules are differentiated from remaining water molecules based on a distance criteria, [Mondal *et al.*, 2020; Srivastava *et al.*, 2020; Debnath *et al.*, 2013]. Water molecules that reside continuously for 100 ps within $\pm 0.35$ nm of the peak location of phosphorous head group density of DMPC lipids are identified as IW. Figure 3.1 (b) and (c) represent the snapshot of IW for hydration number 45 and 4 respectively.

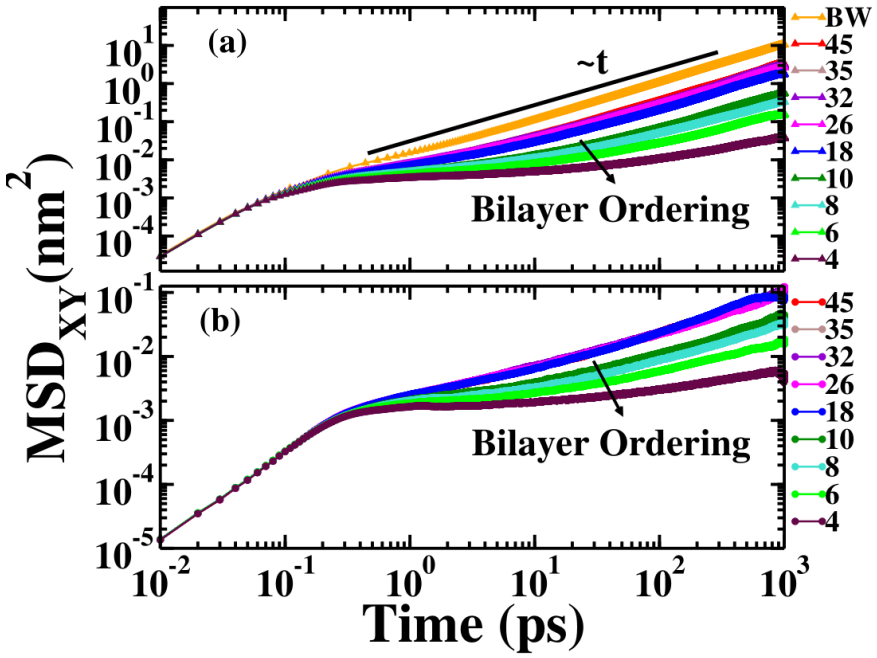


**Figure 3.11 :** Mean square displacements of a) IW and b) phosphorous heads of lipids along xy from hydration number 45 to 4. A prominent slow-down in $MSD_{XY}$ has been observed for both IW and P from $\omega = 10-4$ once the bilayer starts ordering.

### *Translational mean square displacement*

To investigate the influence of dehydration on water dynamics and to find out its relation to bilayer fluid-to-gel crossover, two dimensional (2D) translational mean square displacements ($MSD_{XY}$) of IW and lipid heads are calculated along xy surface for different hydration numbers using the following equation,

$$< r^2(t) >= \frac{1}{N}\sum_{i=1}^{N} < [r_i(t+t') - r_i(t')]^2 >_{t'}, \tag{3.8}$$

where N represents number of molecules, $t'$ is time origin and $t$ is the difference in time. The angular bracket represents average over time origins, $t'$. $MSD_{XY}$ for the BW enters the diffusive regime ($\sim t$) within $0.3-0.4$ ps (figure 3.11 a)). As water contents are lowered, $MSD_{XY}$ of the IW start decreasing and follow sub-diffusive behavior. Similar slow-down in water dynamics with lowering in water content has been observed in earlier experiments [Gruenbaum and Skinner, 2011; Zhao *et al.*, 2008; Mondal *et al.*, 2020; Wassall, 1996] and computational studies [Mondal *et al.*, 2020; Zhang and Berkowitz, 2009; Calero *et al.*, 2016; Högberg and Lyubartsev, 2006; Calero and Franzese, 2019]. The slow-down in $MSD_{XY}$ of the IW upon lowering in $\omega$ is more prominent from $\omega = 10-4$. At $\omega = 4$, the $MSD_{XY}$ of the IW develops a plateau. Similar trend in $MSD_{XY}$ is followed by lipid heads at different $\omega$ as shown in figure 3.11 b). The plateau in $MSD_{XY}$ indicates an emergence of dynamical heterogeneity at low hydration.

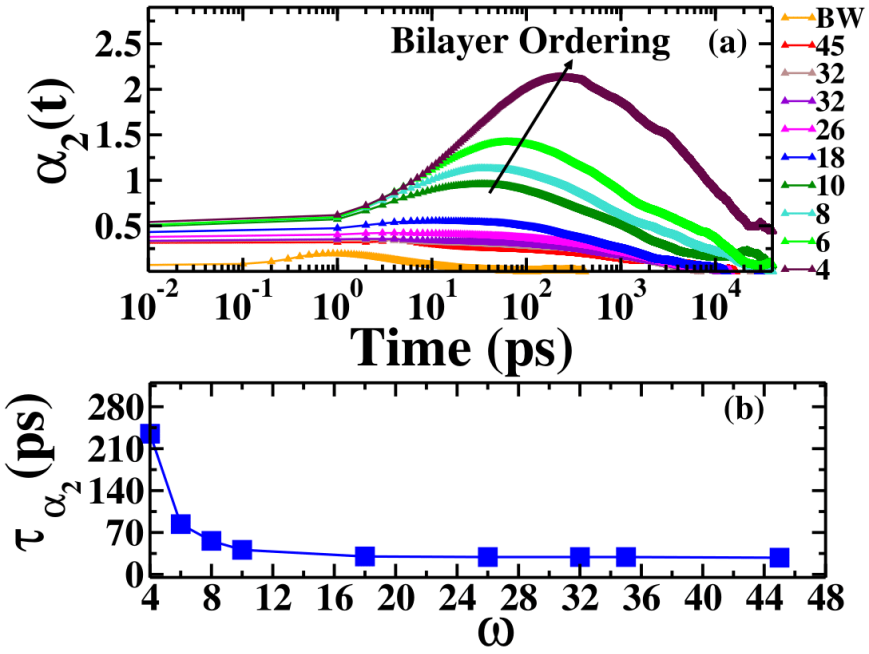


**Figure 3.12 :** (a) non-Gaussian parameter (NGP, $\alpha_2(t)$) as a function of time and (b) changes in relaxation time scales ($\tau_{\alpha_2}$) with respect to the hydration numbers, $\omega$. NGP shows a crossover at the onset of bilayer ordering.

***non-Gaussian parameter***

To check the existence of dynamical heterogeneity in IW due to dehydration, 2D non-Gaussian parameter (NGP) is calculated by [Rahman, 1964],

$$\alpha_2(t) = \frac{< \triangle r(t)^4 >}{2 < \triangle r(t)^2 >^2} - 1. \tag{3.9}$$

$\alpha_2(t) = 0$, if NGP is truely a Gaussian, where, $\triangle r(t) = r(t_0 + t) - r(t_0)$ is particle displacement after a time interval $t$ and angular bracket represents ensemble averaging.

For the BW, NGP increases till $\sim$ 1 ps and then starts decreasing and by 20 ps the NGP of the BW becomes zero as shown in figure 3.12 (a). This relaxation time for the BW is in good agreement with the previously reported time scale for the TIP4P/2005 water model [Srivastava *et al.*, 2019a] and neutron scattering experiments [Arbe *et al.*, 2016]. After 20 ps, the BW molecules show Gaussian dynamics and gradually enter in the diffusive region. For the IW molecules, the values of NGP are initially non-zero and slowly decrease to zero after 70 ns. Similar dynamical heterogeneity has been observed earlier for the IW hydrogen bonded to lipid head groups of a bilayer at room temperature [Srivastava *et al.*, 2019a, 2020]. The peak-heights of the NGPs increase once the water contents are lowered. The amplitude of the NGP increases significantly for the IW near the bilayer with $\omega$ from $10-4$ in association with the bilayer ordering. The NGP of the IW near the bilayer with $\omega = 4$ has the highest peak manifesting the presence of significant amount of dynamical heterogeneity in the IW.

$\beta$ to $\alpha$ relaxation time-scales of the NGP are identified from the locations of their peaks and referred to as $\tau_{\alpha_2}$. As $\omega$ decreases, $\tau_{\alpha_2}$ increases and for $\omega = 4$, there is a drastic increment in $\tau_{\alpha_2}$ (figure 3.12 b). $\beta$ to $\alpha$ relaxation time-scales signify the correlation time-scale of spatially heterogeneous dynamics and feature the cross-over from cage to diffusive time-scale for Brownian particles in a periodic effective field and polymer melts [Starr *et al.*, 2013; Donati *et al.*, 1998]. This clearly shows at the dehydrated state, the IW molecules undergo a strong structural arrest and remain in the cage for much longer time compared to the ones at fully hydrated states. Thus, at lower hydration (from $\omega = 10$ till 4), the IW molecules exhibit glassy dynamics similar to supercooled liquids while the BW molecules follow Fickian dynamics [Das *et al.*, 2020].

### *van Hove correlation function*

Since NGP of the IW shows characteristics of glassy dynamics, self part of one dimensional (1D) van-Hove correlation function is calculated using the equation below,

$$G_s(\mathbf{r},t) = \frac{1}{N}\left\langle \sum_{i=1}^{N} \delta(\mathbf{r} + \mathbf{r}_i(0) - \mathbf{r}_i(t) \right\rangle. \tag{3.10}$$

$G_s(\mathbf{r},t)$ are determined at time, $t = 0.32$ ps for the BW. Figure 3.13 a) represents $G_s(\mathbf{r},t)$ for the BW and the IW with various hydration numbers. The BW molecules follow a Gaussian distribution confirming the Fickian dynamics in the diffusive regime which is in good agreement with the respective $\mathrm{MSD}_{XY}$. $G_s(\mathbf{r},t)$ for the IW are calculated at the time shown in table 3.4 when the IW show sub-diffusive behavior. $G_s(\mathbf{r},t)$ for the IW become prominently non-Gaussian as the hydration numbers are lowered. Similar Gaussian to non-Gaussian transition in van Hove correlation function has been observed for the lipid heads with lowering in water contents in figure 3.13 b). The non-Gaussian nature of van Hove correlation function is known to be the universal feature of dynamical heterogeneity in supercooled liquids [Hove, 1954; Kegel and van Blaaderen, 2000; Puertas *et al.*, 2004; Chaudhuri *et al.*, 2007; Jaiswal *et al.*, 2015]. The non-Gaussianity in van Hove correlation function shows the underlying dynamics to be non-diffusive. Such non-diffusive dynamics has been observed earlier for water assisted conformational transitions of proteins. This demonstrates that at lower hydration, both lipid and IW molecules start exhibiting dynamical heterogeneity with exponential tails in $G_s(\mathbf{r},t)$ and such deviations from Gaussianity is most prominent for the lowest hydration state, $\omega = 4$. Thus dehydration induces dynamical heterogeneity in the IW which results in dynamical heterogeneity in the lipid bilayer facilitating formation of gel bilayers seen in figure 3.8.

### *Self intermediate scattering function*

Self intermediate scattering function (SISF) is another universal feature of dynamical heterogeneity. Since the bilayer is symmetric along xy surface, two dimensional SISF is calculated by following equation,

$$F_s(q,t) = \frac{1}{N}\left\langle \sum_{i=1}^{N} Cos(\mathbf{q}.[\mathbf{r}_i(t) - \mathbf{r}_i(0)]) \right\rangle. \tag{3.11}$$

where, $q = \frac{2\pi}{\lambda}$ and $\lambda$ is the wavelength. $\lambda = 0.50$ nm is chosen for the calculations of SISF as the first peak of $g(r)$ of IW and phosphorous heads are at 0.3 nm and 0.6 nm respectively figure 3.14.

Figure 3.15 shows the SISF of the BW and the IW near bilayers with $\omega = 45$ to 4. The BW decays to zero within 10 ps whereas IW molecules for bilayers with different $\omega$ have much

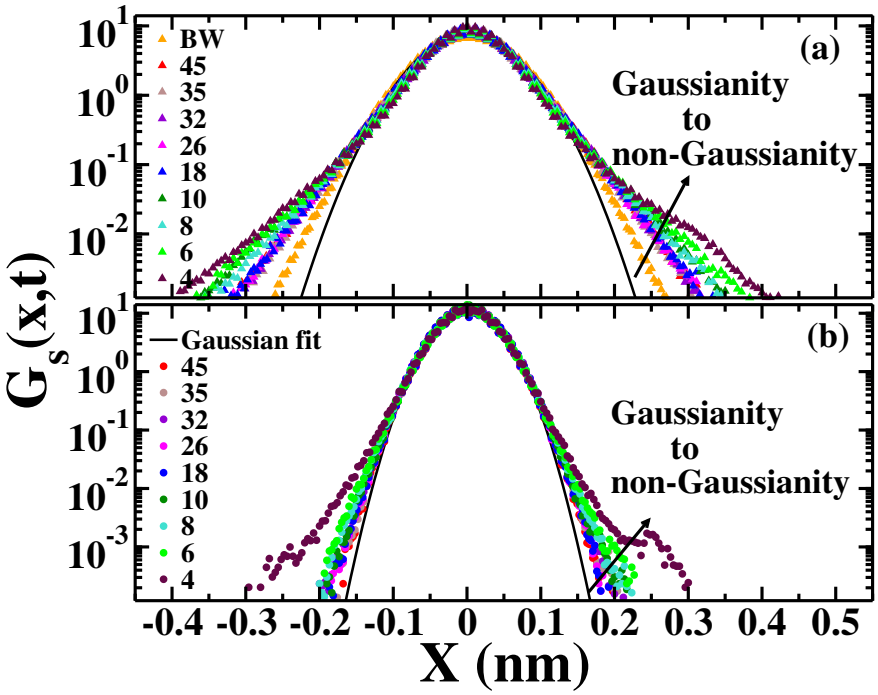


**Figure 3.13 :** Translational 1D van Hove correlation function of a) IW and b) phosphorous (P) heads from hydration number 45 to 4. The distributions are more non-Gaussian in nature for both IW and P at $\omega = 4$.

**Table 3.4 :** Time-scales for van-Hove correlation functions of IW for different hydration numbers.

| $\omega$ | $t$(ps) |
|---|---|
| 45 | 0.61 |
| 35 | 0.62 |
| 32 | 0.62 |
| 26 | 0.64 |
| 18 | 0.72 |
| 10 | 2.01 |
| 8 | 2.31 |
| 6 | 4.93 |
| 4 | 23.80 |

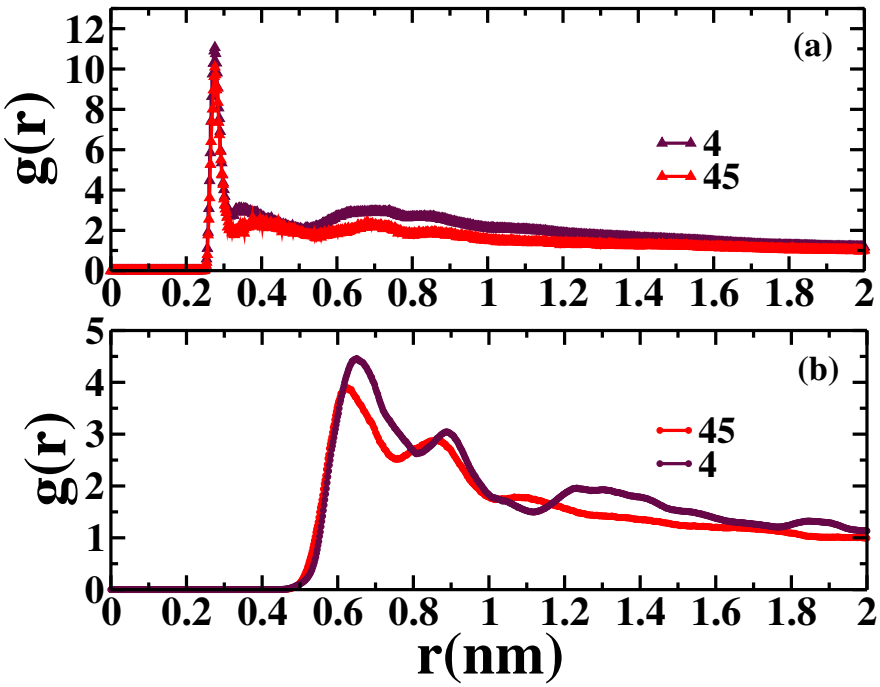


**Figure 3.14 :** $g(r)$ of a) IW and b) phosphorous atoms at hydration number 45 and 4.

slower relaxations compared to the BW. With lowering in water content, relaxation time-scales of the SISF of the IW molecules increase. The relaxation is significantly slow once $\omega$ goes below 18. At $\omega = 4$, $\beta$ and $\alpha$ relaxations are separated by a weak boson peak as seen for supercooled liquids [Hansen and McDonald, 2013].

The $\alpha$ relaxation time-scales ($\tau_\alpha$) are extracted for all cases when the SISF reaches the value of $1/e$, i.e., $F_s(q,t) = 1/e$. Since the SISF of the IW near the bilayer with $\omega = 4$ does not reach $1/e$ within 1 ns, the run-length of the bilayer is extended till 5 ns. Numerical values of the $\tau_\alpha$ calculated for the IW molecules near the bilayers with different hydration numbers, $\omega$, have been mentioned in table 3.6. The slow-down in $\alpha$ relaxation time with lowering in water content shows that cage relaxations of IW molecules take longer time due to dehydration.

To find out a relation between $\tau_\alpha$ and two dimensional diffusion co-efficient, $D$ of IW, $D$ has been obtained from the long time limit of $\mathrm{MSD}_{XY}$ by following Einstein's relation,

$$D = \lim_{t\to\infty} < r^2(t) > /(4t). \tag{3.12}$$

The value of $D$ of the BW from our simulation has been found to be $2.346 \pm 0.026 \times 10^{-5} \mathrm{cm^2 s^{-1}}$ which is in good agreement with previously performed simulation [Srivastava *et al.*, 2019a] and experiment [Holz *et al.*, 2000]. The values of $D$ of the IW at $\omega$ 35 and 4 from our simulations using TIP4P/2005 model are $1.46 \pm 0.01 \times 10^{-5}$ $\mathrm{cm^2 s^{-1}}$ and $0.0284 \pm 0.0029 \times 10^{-5}$ $\mathrm{cm^2 s^{-1}}$ respectively. These values are slightly lower than the previously reported simulations [Calero *et al.*, 2016] using TIP3P water model as TIP3P water model is known to have faster diffusion than TIP4P/2005 water model [Srivastava *et al.*, 2019a].

It is well known that a Brownian particle follows Stokes-Einstein's relation, $D \sim \tau_\alpha^{-1}$ at

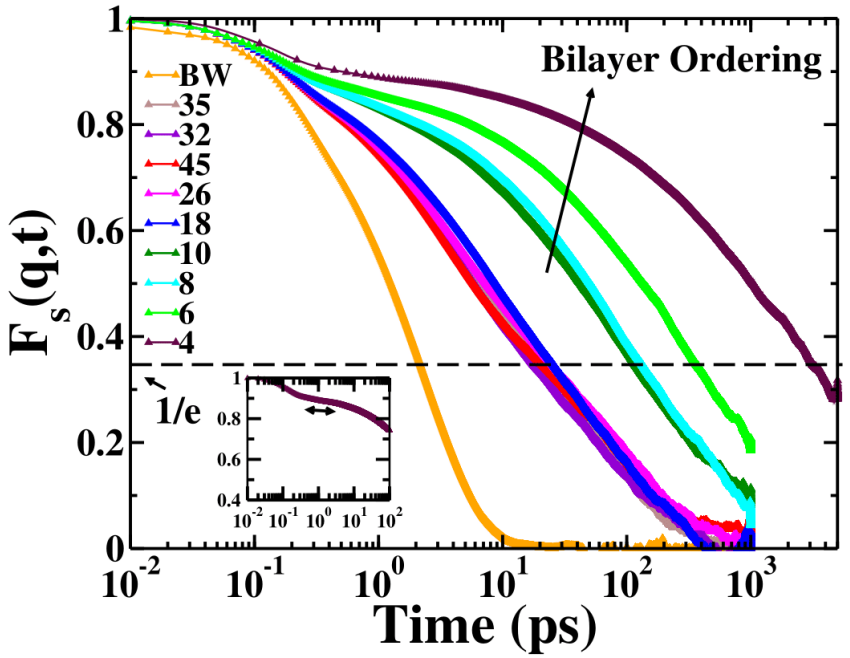


**Figure 3.15 :** SISF of IW for bilayers with $\omega = 45$ to 4 at $\lambda = 0.5$ nm. Dashed line shows the value of $F_s(q,t) = 1/e$ to extract $\tau_\alpha$. Inset shows very weak boson peak for $\omega = 4$.

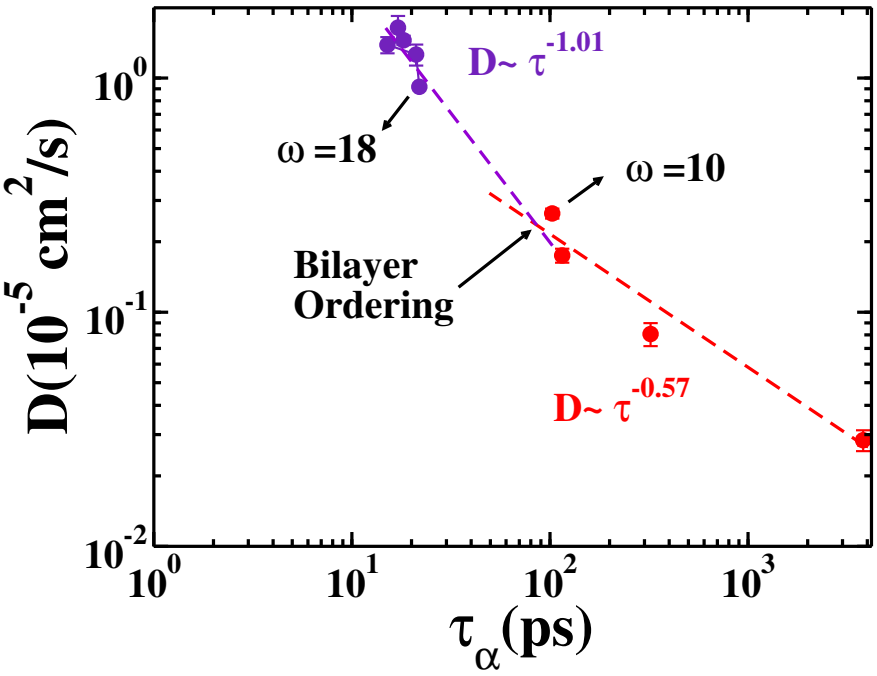


**Figure 3.16 :** Diffusion constant, $D$ vs $\tau$ showing a dynamical crossover near $\omega = 10$. The crossover is associated with bilayer ordering.

room temperature. The relation changes to fractional Stokes-Einstein's relation, $D \sim \tau_\alpha^{-\nu}$, where the scaling component, $\nu < 1$ if the particles follow glassy behavior at lower temperature [Staley *et al.*, 2015; Sengupta and Karmakar, 2014; Viot *et al.*, 2000; Xu *et al.*, 2006; Rössler, 1990]. Experimental evidence of breakdown in Einstein's relation is found for supercooled confined water near a nano-pore or protein or methanol diluted bulk water using NMR and Quasi-Elastic Neutron Scattering spectroscopies [Chen *et al.*, 2006b; Mallamace *et al.*, 2010]. In a binary harmonic sphere mixture of model glass forming liquids, a breakdown of Stokes-Einstein relation accompanied by a dynamic cross-over in $\alpha$-relaxation time with dynamic correlation length, is found below and above mode-coupling temperature [Flenner and Szamel, 2013]. Therefore, to investigate the changes in the IW dynamics due to dehydration, $D$ is plotted with respect to $\tau_\alpha$.Figure 3.16 shows that the relation between $D$ and $\tau_\alpha$ of the IW follows Stokes-Einstein like relation from $\omega = 45$ to 18. The relation breaks to fractional Stokes-Einstein like relation where $\nu \sim 1$ changes to $\nu = 0.57$ from $\omega = 10-4$. Similar change in the scaling exponent has been observed when pinning concentration is increased in a randomly pinned glass forming liquids at constant higher temperature [Li *et al.*, 2015] demonstrating different dynamics at low and high pinning concentrations. As breakdown in Stokes-Einstein relation indicate a cross-over in dynamics [Chen *et al.*, 2006b; Mallamace *et al.*, 2010] and an emergence in dynamical heterogeneity [Li *et al.*, 2015], the change in the scaling exponent found in our work suggests the IW molecules behave similar to glass-forming liquids once the water contents near the bilayer are from $\omega = 10-4$. Interestingly the change in $\nu$ in the IW is associated with the bilayer ordering (figure 3.8) for the same water content. This implies that dynamical heterogeneity in the IW due to the dehydration results in bilayer ordering.

#### *Hydrogen bond auto-correlation functions*

To understand the physical origin of dynamical heterogeneity due to dehydration, hydrogen bond auto-correlation functions (HBACF, $C_{HB}(t)$) is calculated using the following equation [van der Spoel *et al.*, 2006; Luzar and Chandler, 1996a; Chandra, 2000]:

$$C_{HB}(t) = \frac{< h_{IW}(0) h_{IW}(t) >}{< h_{IW} >}, \tag{3.13}$$

where, $h_{IW}(t)$ denotes hydrogen bonds among the BW or the IW. $h_{IW}(t)$ will be 1 if there is a hydrogen bonding else it will be 0.

The hydrogen bonds are allowed to break and reform and thus $C_{HB}(t)$ represents the intermittent hydrogen bond auto-correlation function. The probability of a specific hydrogen bond remains intact, is zero at equilibrium in a large system. Thus $C_{HB}(t)$ relaxes to zero at equilibrium. The HBACF of the BW decays fastest compared to that of the IW as seen from figure 3.17 similar to the previous observations [Luzar and Chandler, 1996a; Srivastava and Debnath, 2018; Calero and Franzese, 2019]. HBACFs of the IW molecules remain correlated significantly for a longer time from $\omega = 10-4$ when the bilayer starts ordering. The HBACFs of the IW is slowest for the lowest $\omega = 4$ suggesting the hydrogen bond dynamics is most hindered for the IW molecules with the lowest $\omega$. Reactive flux analysis has been used to understand the kinetics of hydrogen bond formation or breaking [van der Spoel *et al.*, 2006; Luzar and Chandler, 1996b; Luzar, 2000]. The rate of relaxation ($K(t)$) of $C_{HB}(t)$ to equilibrium is calculated by,

$$K(t) = -\frac{dC_{HB}(t)}{dt}. \tag{3.14}$$

$K(t)$ can be expressed in terms of the forward rate constant ($k$) and the backward rate constant ($k'$) as follows,

$$K(t) = kC_{HB}(t) - k'n(t). \tag{3.15}$$

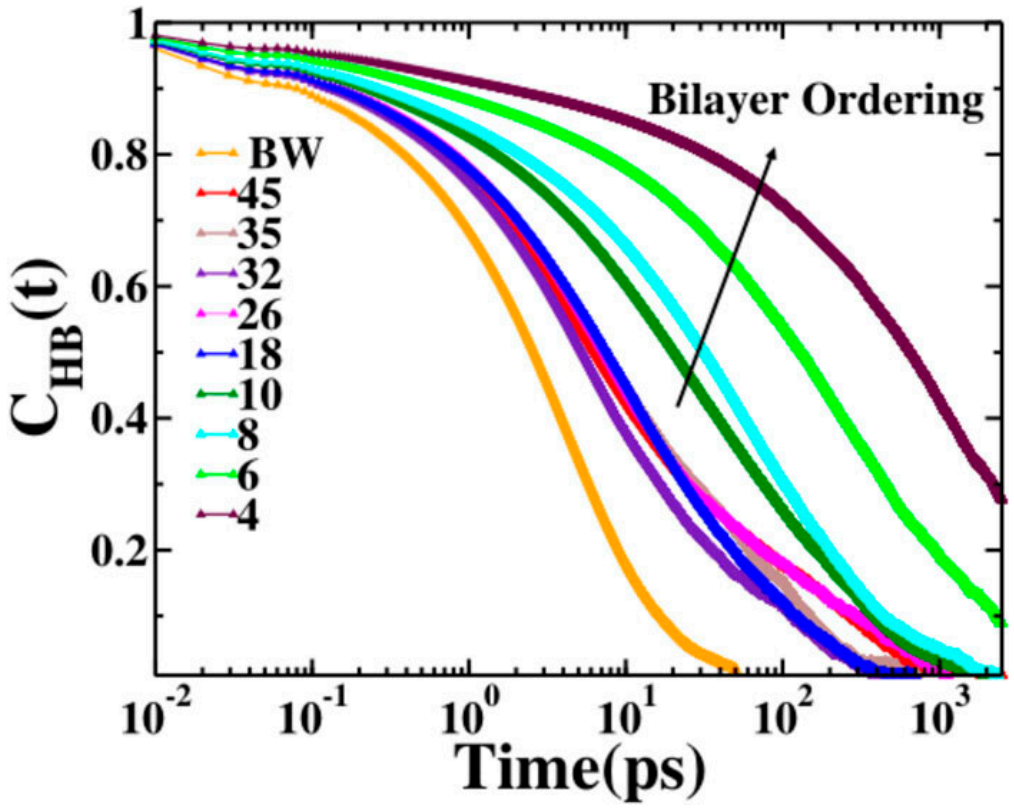


**Figure 3.17 :** Hydrogen bond auto-correlation function of BW and IW near bilayers with different $\omega$ from 45 to 4.

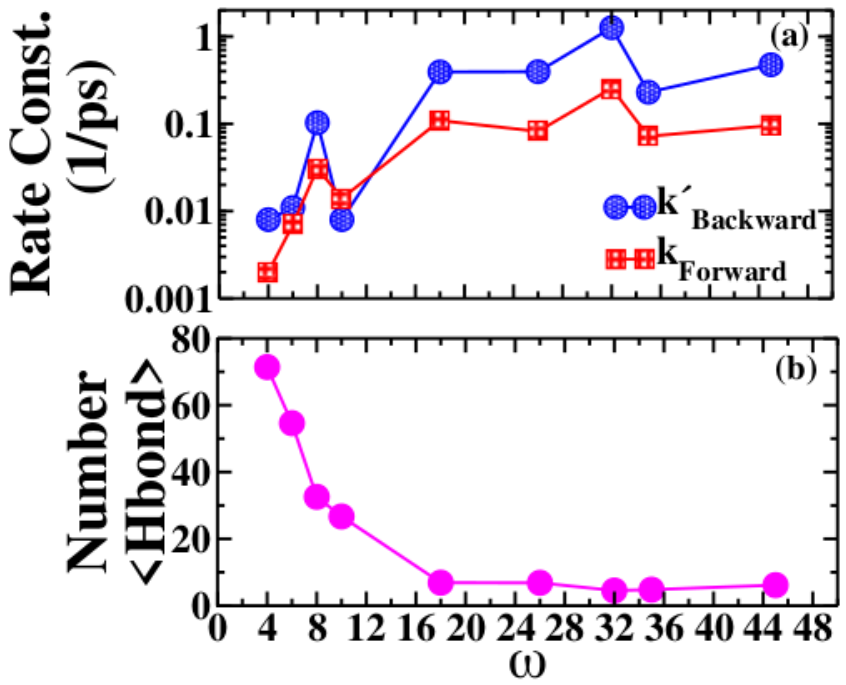


**Figure 3.18 :** (a) Kinetic parameters, $k$ (forward) and $k$‘ (backward) rate constants (for equation 15), (b) Number of average hydrogen bonds shown with respect to $\omega$.

**Table 3.5 :** Number of IW molecules with hydration numbers.

| $\omega$ | Number of IW molecules |
|---|---|
| 45 | 99 |
| 35 | 101 |
| 32 | 102 |
| 26 | 103 |
| 18 | 105 |
| 10 | 180 |
| 8 | 186 |
| 6 | 213 |
| 4 | 256 |

Here $n(t)$ represents the population of broken hydrogen bonds that was present at $t = 0$. Note these hydrogen bond partners may still reside within the hydrogen bond distance. The kinetic parameters, $k$ and $k'$, are shown with respect to $\omega$ in figure 3.18. Both the hydrogen bond breaking (forward) and formation (backward) rate constants of the interface water show a crossover near $\omega = 10$. Since the number of interface water molecules increase upon lowering the hydration number table 3.5, the numbers of average hydrogen bonds follow similar trend figure 3.21. Using the forward rate constant ($k$), the life time of hydrogen bonding is calculated by

$$\tau_{HB(RFA)} = \frac{1}{k}. \tag{3.16}$$

Numerical values of the $\tau_{HB(RFA)}$ calculated using reactive flux analysis (RFA) for the IW molecules near the bilayers with different hydration numbers have been mentioned in table 3.6. Since the forward rate constants decrease with lowering the hydration numbers, $\tau_{HB(RFA)}$ increase upon dehydration. The values of $\tau_{HB(RFA)}$ are compared with the hydrogen bond life times ($\tau_{HB(1/e)}$) obtained from $1/e$ values of $C_{HB}(t)$.

#### *Behavior of relaxation times with hydration numbers*

To investigate the behavior of different relaxation times of the IW due to the change in the hydration numbers, the $\alpha$ relaxation times ($\tau_\alpha$) extracted from $F_s(q,t)$ are compared with the hydrogen bond lifetimes calculated using both methods of reactive flux analysis (RFA) and $1/e$. These time-scales have been plotted with respect to $\omega$ in figure 3.19. The nature of the $\tau_{HB(RFA)}$ and $\tau_{HB(1/e)}$ with respect to $\omega$ shows the comparison of $\omega$ dependence of hydrogen bond lifetimes from both methods. The growing relaxation timescales of $\tau_{HB(RFA)}$ and $\tau_{HB(1/e)}$ towards the lower hydration shows that the hydrogen bonds of the IW remain intact for a significantly longer period of time from $\omega = 10-4$. Similar longer hydrogen bond lifetime for the dehydrated state of DMPC bilayer is reported earlier [Calero *et al.*, 2016]. Interestingly the relaxation timescales of $\tau_\alpha$ and $\tau_{HB}$ follow similar crossovers near $\omega = 10$. This indicates that the nature of the $\alpha$ relaxation times of IW can be reflected in the hydrogen bond lifetimes. This suggests that the hydrogen bond dynamics are the physical origin of long time relaxations obtained from the $F_s(q,t)$. In a previous work, chemically confined IW molecules near a fluid bilayer are found to exhibit similar characteristics [Srivastava *et al.*, 2019a].

The relaxation times versus different hydration numbers in figure 3.19 can be fitted by the Vogel-Fulcher-Tamman (VFT) [Cammarota and Biroli, 2012; Kob and Coslovich, 2014; Li *et al.*,

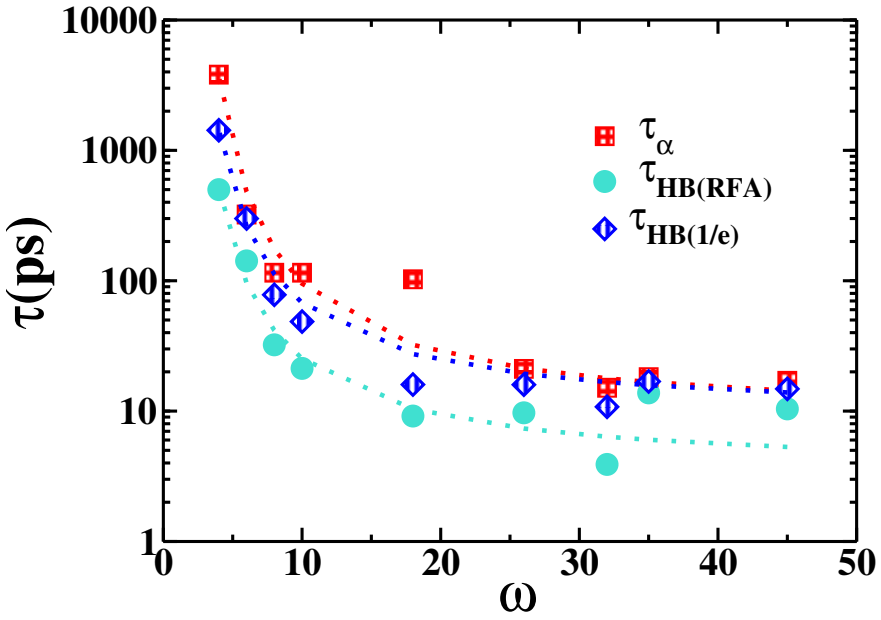


**Figure 3.19 :** Changes in relaxation time scales, $\tau$ with respect to the hydration numbers, $\omega$. $\tau_\alpha$ obtained from $F_s(q,t)$ and $\tau_{HB}$ obtained from both reactive flux analysis (RFA) and $1/e$ value of $C_{HB}(t)$ follow similar crossovers from $\omega = 10-4$.

2015] like equation given below,

$$\tau = \tau_0 exp\left(\frac{K\omega_0}{\omega - \omega_0}\right) \tag{3.17}$$

Here, $\omega_0$ quantifies the hydration number characterising a fluid-to-gel crossover in the bilayer, $K$ is the fragility parameter. The fitting parameters in table 3.7 shows that the characteristic hydration number is $\omega \sim 10$ at which the bilayer transforms from a fluid/ripple like phase to a gel-like phase. This result is in agreement with figure 3.16 and with all our calculations which indirectly show that the bilayer starts ordering from $\omega \sim 10$. Below 10 the bilayer remains in an ordered or gel like state. At the onset of the bilayer ordering, there is an emergence of dynamical heterogeneity in the IW molecules near the bilayer.

### *Reorientational auto-correlation function (RACF)*

To understand the influence of hydration numbers on the rotational dynamics of water, reorientational auto-correlation function (RACF) is calculated for the IW for different hydration numbers and the BW. The RACF, $C_{vl}(t)$, of water is calculated by the following equation,

$$C_{vl}(t) = \frac{< \sum_{i=1}^{N} P_l[e_i{}^v(t) \cdot e_i{}^v(0)] >}{< \sum_{i=1}^{N} P_l[e_i{}^v(0) \cdot e_i{}^v(0)] >} \tag{3.18}$$

where, $e_i{}^v(t)$ represents the vector for which the RACF is calculated and $P_l$ is the $l^{th}$ order Legendre polynomial. $C_{vl}(t)$ are computed for the first ($l = 1$) and the second order ($l = 2$) Legendre polynomial for the OH bond vector ($\vec{OH}$), the HH bond vector ($\vec{HH}$) and the dipole moment vector $\vec{\mu}$. Figure 3.20 a) and b) shows that the RACF for the first and second order Legendre polynomials

**Table 3.6 :** The relaxation timescales obtained for different $\omega$.

| $\omega$ | $\tau_\alpha$ (ps) | $\tau_{HB(RFA)}$ (ps) | $\tau_{HB(1/e)}$ (ps) |
|---|---|---|---|
| 45 | 17.09 | 10.4 | 14.8701 |
| 35 | 18.23 | 13.8 | 16.89 |
| 32 | 15.11 | 3.9 | 10.79 |
| 26 | 21.09 | 9.71 | 15.95 |
| 18 | 102.64 | 9.71 | 15.95 |
| 10 | 115.23 | 21.27 | 15.99 |
| 8 | 115.23 | 32.25 | 78.04 |
| 6 | 322.13 | 142 | 300.14 |
| 4 | 3812 | 500 | 1426.11 |

**Table 3.7 :** VFT fitting parameters.

| $\tau$ | $\tau_0$ (ps) | $K$ | $\omega_0$ |
|---|---|---|---|
| $\tau_\alpha$ | 327460 | 2.3 | 10.47 |
| $\tau_{HB(1/e)}$ | 198728 | 2.03 | 10.02 |
| $\tau_{HB(RFA)}$ | 80000 | 2.01 | 10.1 |

respectively for the IW and the BW.

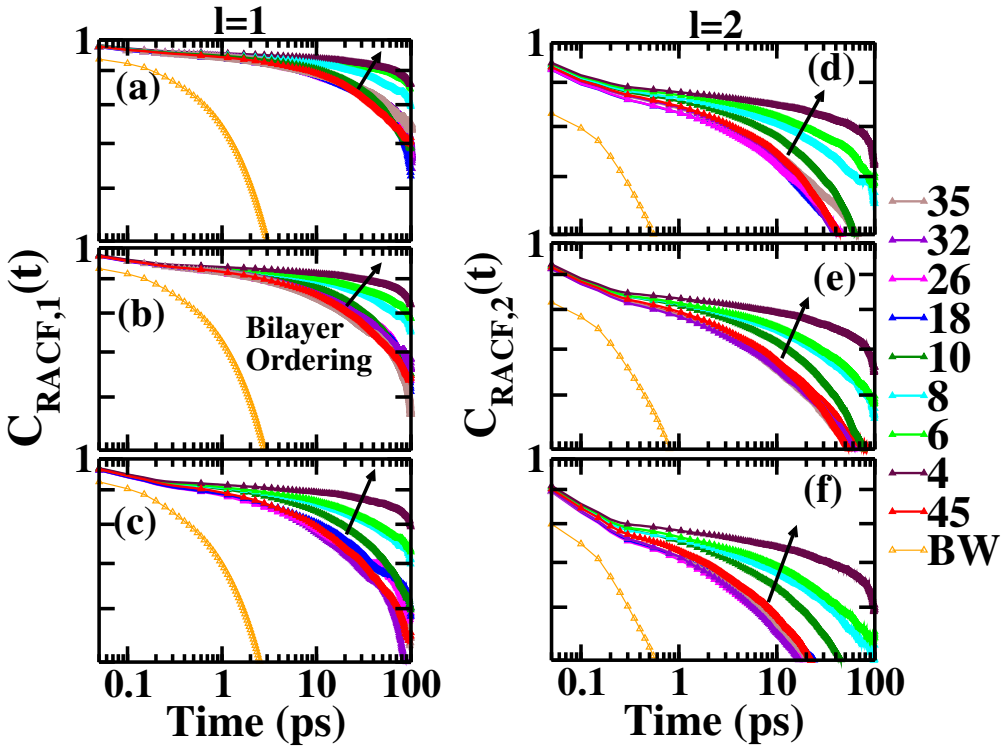


**Figure 3.20 :** RACF of the IW and bulk water for $\vec{OH}$ (a and d), $\vec{HH}$ (b and e) and $\vec{\mu}$ (c and f) for $l = 1$ and 2.

The RACFs of the BW much rapidly decay to zero compare to that of the IW showing a faster relaxation to the equilibrium. The $C_{v2}(t)$ decreases faster than the $C_{v1}(t)$ for all cases. Both $C_{v1}(t)$ and $C_{v2}(t)$ for all cases exhibit slower decay as hydration number decreases. The RACF for the IW water for the $\omega = 45$ to 18 overlap with each other showing no difference in orientations. The RACF of the IW significantly differ from $\omega = 10$ onwards at the onset of the bilayer ordering. The most preferred orientations of the IW are obtained at $\omega = 4$ for all cases. Similar slowdown in the rotational relaxation has been observed in water near DMPC and DLPC bilayers [Zhang and Berkowitz, 2009; Calero *et al.*, 2016]. The preferred orientations of the IW for the lower $\omega$ is attributed to the persistent hydrogen bonds with longer lifetime. Earlier calculations suggest that the probability of hydrogen bonds between IW and lipid increases as the hydration number decreases and most of the water reside in the interior of the membrane [Calero *et al.*, 2016]. Upon dehydration, bound water bridging lipids increases with longer lifetime of lipid-water hydrogen bonds. At the same time, fraction of the lipid unbound water decreases. Since the structure of bound and unbound water to the lipids are different due to hydrogen bond network and coordination defects, residence time of bound water increases changing the lipid mobility and membrane fluctuations. The significant slowdown in the RACF of the IW in association with the bilayer ordering indicate a coupling between the rotational dynamics of the IW with the bilayer phase change.

### *Dynamics of the lateral organization of the bilayer*

Two dimensional (2D) van Hove correlation function of lipid phosphorous head is calculated by the following equation[Shafique *et al.*, 2016]:

$$G_s^{simulation}(\mathbf{r},t) = \frac{1}{N}\left\langle \sum_{i=1}^{N} \delta(\mathbf{r} + \mathbf{r}_i(0) - \mathbf{r}_i(t) \right\rangle. \tag{3.19}$$

Here, $r$ is the displacement of phosphorous head of the lipid at time $t$. The calculation is done for a 40 ns run-length. It is well known that the van Hove correlation function of the Brownian particles should obey a Gaussian distribution. Thus, to measure the deviations of the 2D van Hove of lipids from that of the Brownian particles, theoretical van Hove correlation function $G^{theory}$ is calculated in two dimensions by the following equation [Dueby *et al.*, 2019],

$$2\pi r G^{theory}(r,t) = \frac{2r}{< r^2(t) >} exp^{\frac{-r^2}{<r^2(t)>}} \tag{3.20}$$

$< r^2(t) >$ is the 2 dimensional mean square displacement along x and y at time $t$. $G_s^{simulation}(r,t)$ and $G_s^{theory}(r,t)$ cross each other at two characteristics distances $r_1$ and $r_2$. These two distances are considered as the cut-offs for the particles which remain within the cage and which undergo jump [Dueby *et al.*, 2019]. If the displacement of a particle, $r < r_1$, the particle is tagged as a particle within a cage. If the displacement of a particle, $r > r_2$, the particle is tagged as a mobile particle. Figure 3.22 shows the simulated and theoretical 2D van Hove correlation functions for the phosphorous heads for different $\omega$. The $G_s^{simulation}(r,t)$ do not deviate much from the $G_s^{theory}(r,t)$ above $\omega = 10$ confirming the fluid phase of the bilayer as seen in figure 3.8. At the onset of the bilayer ordering near $\omega = 10$, the differences between $G_s^{simulation}(r,t)$ and $G_s^{theory}(r,t)$ are much prominent. At $\omega = 4$ the deviations are significant demonstrating the gel phase of the bilayer. Both the cut-off distances, $r_1$ and $r_2$, reduce with lowering in $\omega$ (figure 3.23). The cut-off

$r_1$ ranges between 0.4 to 0.15 nm so that the mean square displacements of mobile lipid heads ($< r^2_{mobile}(t) >^{1/2} = 2r_2$) vary from 0.8 nm to 0.3 nm. The displacements are slightly larger than the inter-molecular spacing $\sim 0.6-0.3$ nm obtained from the location of the first peak of $g(r)$ figure 3.14 or the $\sigma$ value of the non-bonded Lennard-Jones potential. Thus at the onset of bilayer ordering near $\omega = 10$, two distinct classes of mobility groups are found for the bilayer: few lipids remain within the cage cut-off distance $r_1$ and few lipids escape these cages and move beyond the distance of intermolecular spacing suggesting a "molecular replacement mechanism" in lipid dynamics. This feature has been observed earlier for coarse-grained DPPC lipids in gel phase [Shafique *et al.*, 2016]. The fractions of caged and mobile lipids ($f_{cage/mobile}$) are calculated after averaging over 39,000 frames for 40 ns run-lengths using the following equation,

$$f_{cage/mobile} = \frac{< n_{cage/mobile} >}{N}, \tag{3.21}$$

where $< n >$ is the time averaged number of caged or mobile lipids based on the cut-off distances, $r_1$ and $r_2$ respectively, $N$ is the total number of lipids. Table 3.8 represents the fractions of the caged and mobile lipids in bilayers with different hydration numbers. The fraction of caged lipids increase and the mobile lipids decrease with lowering in hydration numbers below 18. At $\omega = 4$, the fraction of the mobile lipids is minimum and the fraction of the caged lipids is more than 50% resulting in an ordered bilayer or a gel phase. Note, for all these cases, there can be another kind of lipids which are neither confined within a cage nor completely mobile after cage relaxations. These distinct mobility groups are not visible for the fluid phase above $\omega = 10$.

**Table 3.8 :** Fractions of caged ($f_{cage}$) and mobile ($f_{mobile}$) lipids with different hydration numbers.

| $\omega$ | $f_{cage}$ (in %) | $f_{mobile}$ (in %) |
|---|---|---|
| 10 | 36.7 | 13.1 |
| 8 | 43.7 | 9.9 |
| 6 | 45.0 | 8.3 |
| 4 | 51.1 | 7.26 |

To visualize the lateral organizations of the bilayers at high and low hydration numbers, phosphorous heads are color coded as caged and mobile particles based on the cut-off distances for a single snapshot. If the displacement of a lipid head remains within the cage at any instant of time, the head is tagged with green color. Similarly if the displacement of a lipid head is greater than $r_2$, the lipid head is considered as a mobile particle and shown in blue. Figure 3.24 (a) shows all particles are mobile (blue) in the fluid phase as there are no distinct mobility groups present. In the gel phase at hydration number 4, the bilayer ( figure 3.24 (b)) has two classes of lipids with $\sim 50\%$ caged particles with strong structural arrest in combination with very few mobile particles. The number of clusters and maximum size of the clusters for caged and mobile lipid heads at different hydrations are calculated. Upon dehydration, the maximum size of the clusters increases for caged lipids and decreases for mobile lipids with an opposing effect on number of clusters figure 3.21 a), b), d) and e). This indicates the growth of the cluster size of caged lipids at the cost of reduction of clusters of mobile lipids on lowering the hydration numbers. Unlike the reported mobile lipids in coarse-grained DPPC lipid gel phase at 300 K [Shafique *et al.*, 2016], the mobile particles do not form any cluster in the present dehydration induced gel phase and are dispersed throughout the bilayer surface indicating no spatial correlation within the mobile lipids. However, the caged lipids stick together forming clusters or continuous nano-domains spanning across the bilayer surface (figure 3.24 b). It is known that the fractal dimension of the largest cluster characterizes the location of a true percolation threshold [Jan, 1999; Pártay *et al.*, 2007; Roy *et al.*, 2011; Roy and Bagchi, 2013]. Percolation transition happens if the fractal dimension reaches a value of 91/48 in

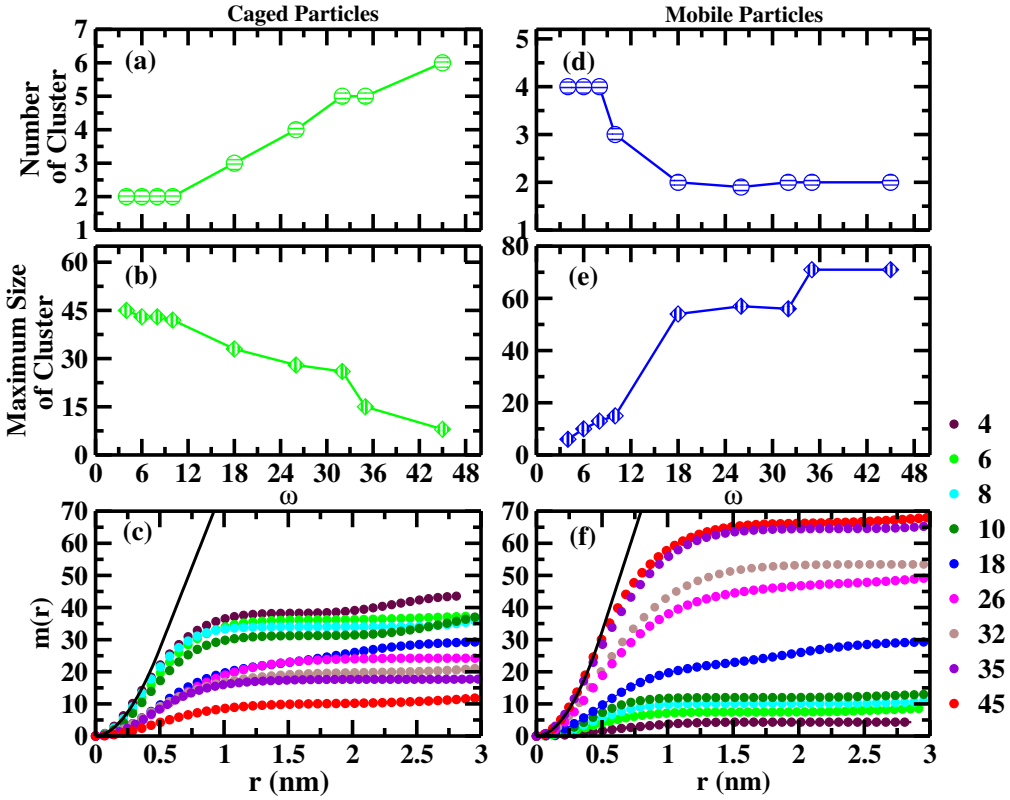


**Figure 3.21 :** Number of clusters of (a) caged and (d) mobile lipid heads, maximum size of clusters of (b) caged and (e) mobile lipid heads, 2-D cumulative radial distribution functions (m(r)) of (c) caged and (f) mobile lipid heads respectively at different hydration numbers. Solid black lines in (c) and (f) show fitting of 4 and 45 respectively.

two dimensions since any object only with fractal dimension greater than 91/48 can be infinite. The fractal dimension of the largest cluster can be calculated from the fitting of the cumulative radial distribution function ($m(r)$ ) as

$$m(r) \sim r^{d_f} \tag{3.22}$$

where $d_f$ is the dimension of the fractal. Figure c) and f) in the 3.21 shows that $m(r)$ of caged and mobile lipids do not follow a scaling relation as in equation (22). The fitted lines to equation (22) are shown in solid black lines in figure 3.21 c) and f). The deviations of the fitted data after 0.5 nm indicates that the clusters of caged lipids may not obey percolation. Similar results have been obtained in three dimensions (data not shown).

## 3.4 CONCLUSIONS

We have investigated the structural and dynamical properties of DMPC lipid bilayers by lowering hydration numbers at 308K using all atom MD simulations. The decrease in area per head group and increase in bilayer thickness superimposed on the bilayer surface and order parameter of lipids upon dehydration clearly demonstrate that the bilayer undergoes moderate structural ordering with a fluid to a gel crossover when hydration number ($\omega$) reduces to 10. The structural properties of the bilayers obtained from our simulations are in good agreement with experimental

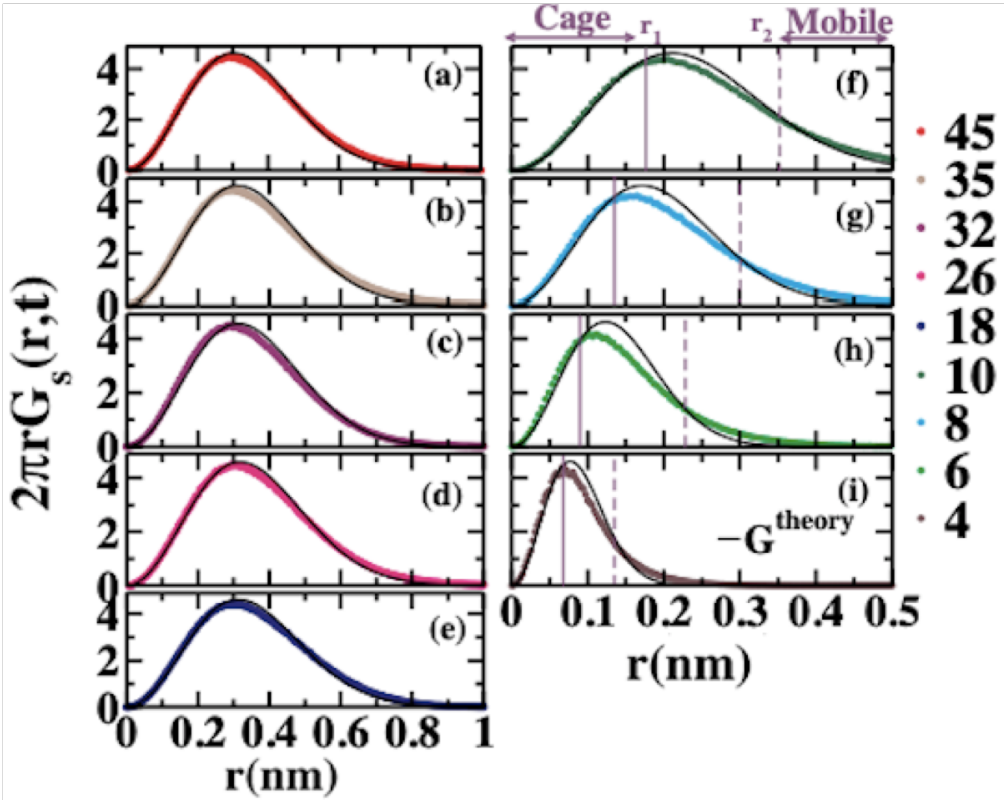


**Figure 3.22 :** 2D van Hove correlation functions for P a) 45 to i) 4, dotted lines - $G_s^{simulation}$, solid black lines - $G_s^{theory}$. Maximum deviation from the Gaussianity has been found at $\omega = 4$. The deviation clearly demonstrates non-Brownian motions in lipid heads due to heterogeneity of lipids in the gel phase.

and simulated values in literature [Stachura *et al.*, 2019; Högberg and Lyubartsev, 2006; Zhuang *et al.*, 2014; Kučerka *et al.*, 2011; Khakbaz and Klauda, 2018; Srivastava *et al.*, 2019b]. In order to understand the role of water in such structural changes of the bilayer, interface water molecules (IW) are identified based on geometric criteria and their residence times. The $MSD_{XY}$ of both the IW and lipid heads show more sub-diffusive behavior on lowering the water contents. The plateau in the $MSD_{XY}$ of the IW at the dehydrated state indicates a possibility of glass-like behavior of the IW at room temperature.

To confirm the presence of glassy behavior of the IW, the non-Gaussian parameters of the IW are calculated for all $\omega$. The $\beta$ to $\alpha$ relaxation times slow down from hydration $10-4$ manifesting the emergence of dynamical heterogeneity in the IW at the onset of bilayer ordering upon dehydration. This is attributed to a strong structural arrest of the IW in a cage for longer time at lower water contents. 1D van Hove correlation functions of both the IW and phosphorous head atoms exhibit significant non-Gaussianity manifesting non-diffusive behavior of both the IW and the lipid heads at lower water contents. To obtain the structural relaxation of the IW, SISF is calculated for the IW near the bilayers with different hydration numbers. Relaxations of the SISF of the IW slow down on approaching lower water contents. At the dehydrated state ($\omega = 4$), a very weak boson peak indicated by a small region of plateau separating the $\beta$ and $\alpha$ relaxations in the SISF of the IW has emerged. Similar boson peak arises for glass-forming liquids with lowering in temperature [Hansen and McDonald, 2013]. Such a plateau like region in the SISF of the IW with

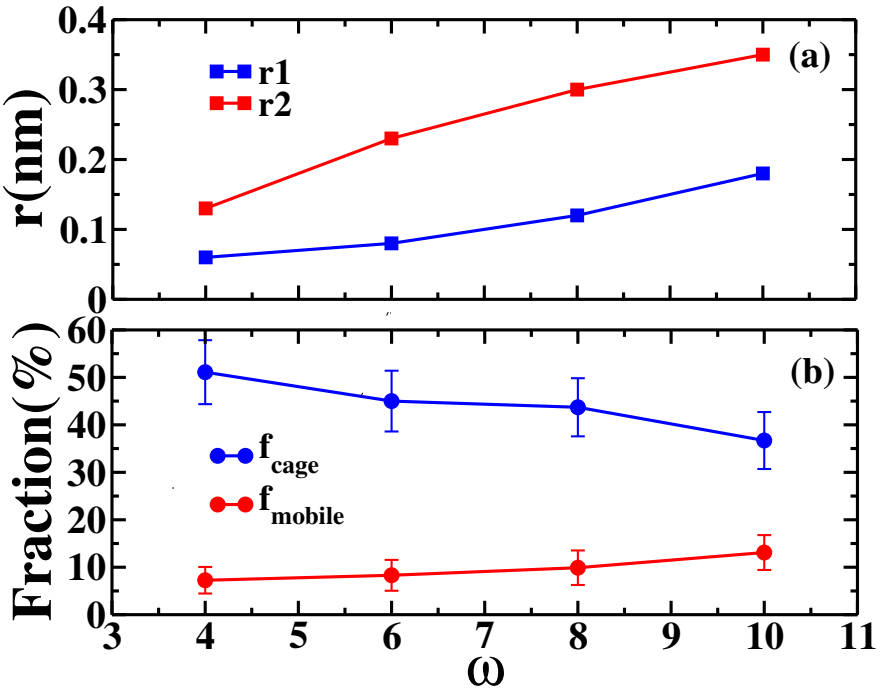


**Figure 3.23 :** a) Cut-off displacements, $r_1$ and $r_2$ versus different hydration numbers, $\omega$ where $r_1$ and $r_2$ represent displacements for the cage and mobile particles respectively, b) fractions of lipids with cage and mobile particles with respect to $\omega$.

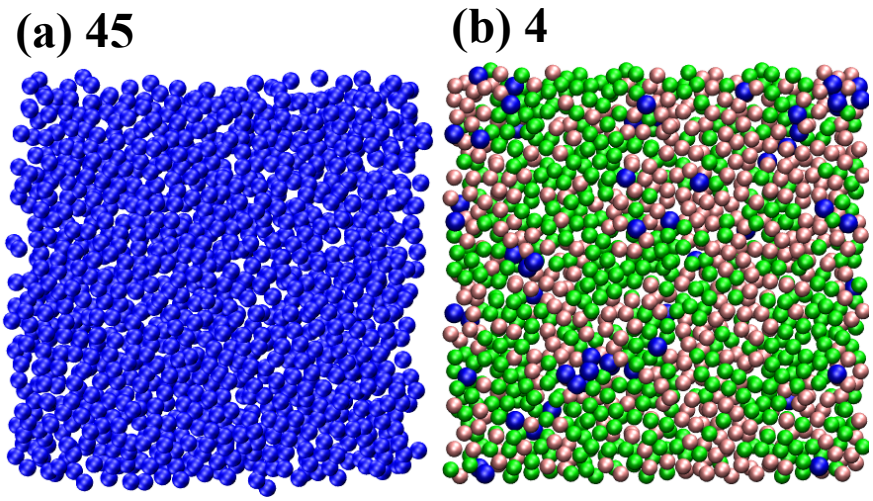


**Figure 3.24 :** Snapshots of mobile and caged atoms in VDW (van der Waals) representations at a) 45 to b) 4. Blue: mobile; green: caged.

respect to time provides a measure of the extent of structural arrest in the IW due to dehydration. The structural relaxation times (obtained from the SISF of the IW slow down with lowering in water contents. The structural relaxation time and the diffusion constant obtained from the linear region of the $MSD_{XY}$ obey Stokes-Einstein's relation as $D \sim \tau_\alpha^{-1}$ at room temperature for the IW above $\omega = 10$. On the onset of the bilayer ordering near $\omega = 10$, a dynamical cross-over in the $\tau_\alpha$ has been observed where $D \sim \tau_\alpha^{-0.57}$. This observation is reminiscent of fractional Stokes-Einstein's

relation found for confined supercooled water using experiments or for binary mixture of model glass-forming liquids [Chen *et al.*, 2006b; Mallamace *et al.*, 2010; Flenner and Szamel, 2013]. This clearly shows that the dehydration in the bilayer induces an emergence of dynamical heterogeneity in the IW in association with bilayer ordering.

To find out the physical origin of the dynamical heterogeneity in the IW, HBACFs are calculated for the IW at different hydration states. The decay in HBACF slows down significantly from $\omega = 10-4$ when the bilayer starts ordering. Using reactive flux analysis, hydrogen bond lifetime $\tau_{HB}$ has been calculated for the IW at different $\omega$. Interestingly, the $\alpha$ relaxation time, $\tau_\alpha$, follows similar behavior as the $\tau_{HB}$ with a rise near $\omega = 10$ suggesting the hydrogen bonds are the physical origin of the $\tau_\alpha$ of the IW. The behavior of both the relaxation times ($\tau_{HB}$ and $\tau_\alpha$) with $\omega$ are fitted to VFT like equation to obtain a characteristics hydration number $\omega = 10$ indicating a cross-over. Note our previous analysis shows that the bilayer undergoes the fluid-to-gel crossover at the same $\omega$. Rotational auto-correlation function, RACF, of the IW are calculated for both the 1st and 2nd order Legendre polynomial. The rotational relaxations of the IW fall off at significantly longer times once the hydration numbers are from $10-4$. A significant slowdown in the rotational relaxation in association with the bilayer ordering indicates a coupling between rotational dynamics of the IW with the bilayer ordering. The preferred orientation of the IW due to longer hydrogen bond lifetime facilitates in shrinkage in area per head group at lower hydration and increase in bilayer ordering. Although, dynamics of the interface water and local lipids are affected strongly due to dehydration in association with bilayer ordering, the structural changes in bilayers are comparatively moderate in nature. This is consistent with previous molecular dynamics findings [Högberg and Lyubartsev, 2006].

To understand the effect of dynamical heterogeneity on the lipid displacements during the fluid-to-gel crossover, 2D van Hove correlation functions of the lipid phosphorous head groups are calculated at different $\omega$. Above $\omega = 10$, the simulated van Hove correlation functions of lipid heads match well with the theoretical van Hove correlation functions for the Brownian particles. The Brownian nature of the displacements of the lipid heads confirms the fluidic, $L_\alpha$ phase of the bilayer above $\omega = 10$. Below this, the simulated van Hove correlation functions of lipid heads deviate from the theoretical ones with two characteristic cut-off distances $r_1$ and $r_2$ both of which decay with lowering in $\omega$. These two cut-offs, $r_1$ and $r_2$ provide spatial measures of cage and mobile particles respectively. At the onset of the bilayer ordering, the fraction of the caged lipid molecules increases with lowering in water content with a decrease in the fraction of the mobile lipid molecules. The mobile lipids move slightly larger than the intermolecular spacing of the lipids suggesting a possibility of existence of molecular displacement mechanism observed earlier for the gel phase of coarse-grained DPPC bilayer [Shafique *et al.*, 2016]. This clearly demonstrates that the spatial distribution of lipid dynamics becomes heterogeneous in nature upon dehydration. In contrast to the previous observation for the gel phase of the coarse-grained DPPC bilayer, no cluster is formed by the mobile particles in the gel phase obtained by the dehydration. Instead the cluster of caged lipids spans all over the bilayer surface. Preliminary results suggest no percolation in the clusters of caged lipids. Such a difference in the spatial distribution of lipid dynamics reveals that the spatio-temporal correlations in the gel phase obtained by the dehydration can be different than those obtained by cooling. The dehydration induces non-Brownian dynamics to the lipids originating from distinct mobility groups which results in formation of the gel phase. Thus the present analysis unfolds the mechanism of fluid-to-gel crossover of bilayer assisted by growing relaxation time-scales of the interface water and dynamical heterogeneity due to the dehydration. This clearly suggests that the structural changes of the bilayers are correlated with the dynamics of the interface water upon dehydration. Similar phenomenon has been observed earlier for surfactant membranes due to lowering in temperature using molecular dynamics simulations

[Debnath *et al.*, 2013]. Thus the present work enhances our fundamental understanding on the membrane dehydration and can help in mimicking cryogenic behavior of membranes at room temperature. Our analyses pave the way of finding controlling parameters to achieve functionally relevant nano-domain formations in complex bio-membranes under anhydrobiosis conditions.

---

**Publication:**
**Malik, S.**; Debnath, A.; Dehydration induced ordering mechanism of lipid bilayers, **J. Chem. Phys. 2021**, 154, 174904